②

NAVAL POSTGRADUATE SCHOOL
Monterey, California

AD-A226 399

DTIC
S ELECTE
SEP 1 3 1990
D
D

THESIS

NONMETALLIC INCLUSIONS
IN
HSLA STEEL WELDMENTS

by

Brent A. Douglas

December, 1989

Thesis Advisor: Alan G. Fox

90

REPORT DOCUMENTATION PAGE

1a. REPORT SECURITY CLASSIFICATION Unclassified		1b RESTRICTIVE MARKINGS	
2a. SECURITY CLASSIFICATION AUTHORITY		3. DISTRIBUTION / AVAILABILITY OF REPORT Approved for public release, distribution is unlimited.	
2b. DECLASSIFICATION / DOWNGRADING SCHEDULE			
4. PERFORMING ORGANIZATION REPORT NUMBER(S)		5. MONITORING ORGANIZATION REPORT NUMBER(S)	
6a. NAME OF PERFORMING ORGANIZATION Naval Postgraduate School	6b. OFFICE SYMBOL (If applicable) 69	7a. NAME OF MONITORING ORGANIZATION Naval Postgraduate School	
6c. ADDRESS (City, State, and ZIP Code) Monterey, CA 93943-5000		7b. ADDRESS (City, State, and ZIP Code) Monterey, CA 93943-5000	
8a. NAME OF FUNDING / SPONSORING ORGANIZATION	8b. OFFICE SYMBOL (If applicable)	9. PROCUREMENT INSTRUMENT IDENTIFICATION NUMBER	
8c. ADDRESS (City, State, and ZIP Code)		10. SOURCE OF FUNDING NUMBERS	

	PROGRAM ELEMENT NO.	PROJECT NO.	TASK NO.	WORK UNIT ACCESSION NO.

11. TITLE (Include Security Classification)

Nonmetallic Inclusions In HSLA Steel Weldments

12. PERSONAL AUTHOR(S)   Douglas, Brent A.

13a. TYPE OF REPORT Master's Thesis	13b. TIME COVERED FROM _____ TO _____	14. DATE OF REPORT (Year, Month, Day) December 1989	15. PAGE COUNT 102

16. SUPPLEMENTARY NOTATION
THE VIEWS EXPRESSED IN THIS THESIS ARE THOSE OF THE AUTHOR AND DO NOT REFLECT THE OFFICIAL POLICY OR POSITION OF THE DEPARTMENT OF DEFENSE OR THE U.S. GOVERNMENT.

17. COSATI CODES			18. SUBJECT TERMS (Continue on reverse if necessary and identify by block number)
FIELD	GROUP	SUB-GROUP	nonmetallic inclusions, HSLA, welding

19. ABSTRACT (Continue on reverse if necessary and identify by block number)

The U.S. Navy is currently funding a program for certification of HSLA steels to replace the HY series of high strength steels for structural fabrication. Integral to this program is the certification of welding consumables for use with these steels. The size, distribution and composition of nonmetallic inclusions in HSLA steel weld metal has been shown to play a key role in the final strength and toughness of the deposited weld. The purpose of this study was to develop a procedure for analysis of nonmetallic inclusions in HSLA steel multipass weldments utilizing optical microscopy and examination and EDX analysis in a SEM. The results of the study suggest that the mean diameter of inclusions in the final pass of a GMAW weldment in a 2.0 inch HSLA-100 plate is larger than the mean diameter of those in the root pass. Additionally the material in the final pass contains a greater amount of Si and Ti deoxidation products than that in the root pass. The larger size, composition and complex structure of the inclusions in the final pass suggest that they contain deoxidation products from previous welding passes which have been released through remelting and coalesced into larger inclusions. (JS)

20. DISTRIBUTION / AVAILABILITY OF ABSTRACT ☒ UNCLASSIFIED/UNLIMITED ☐ SAME AS RPT. ☐ DTIC USERS	21. ABSTRACT SECURITY CLASSIFICATION Unclassified	
22a. NAME OF RESPONSIBLE INDIVIDUAL Alan G. Fox	22b. TELEPHONE (Include Area Code) (408) 646-2586	22c. OFFICE SYMBOL 69Fo

DD FORM 1473, 84 MAR   83 APR edition may be used until exhausted.   SECURITY CLASSIFICATION OF THIS PAGE
All other editions are obsolete

Thesis

Unclassified

Nonmetallic Inclusions
In
HSLA Steel Weldments

by

Brent A. Douglas
Captain, United States Marine Corps
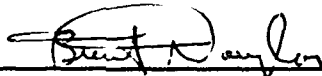B.S., United States Naval Academy, 1981

Submitted in partial fulfillment
of the requirements for the degree of

MASTER OF SCIENCE IN ENGINEERING SCIENCE

from the

NAVAL POSTGRADUATE SCHOOL
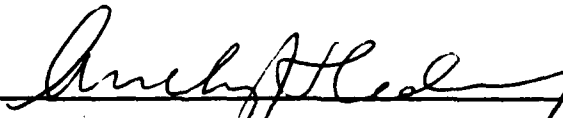December 1989

Author: _____

Brent A. Douglas

Approved by: _____

Alan G. Fox, Thesis Advisor

_____

Indranath Dutta, Second Reader

_____

Anthony J. Healey, Chairman
Department of Mechanical Engineering

ii

ABSTRACT

The U.S. Navy is currently funding a program for certification of HSLA steels to replace the HY series of high strength steels for structural fabrication. Integral to this program is the certification of welding consumables for use with these steels. The size, distribution and composition of nonmetallic inclusions in HSLA steel weld metal has been shown to play a key role in the final strength and toughness of the deposited weld. The purpose of this study was to develop a procedure for analysis of nonmetallic inclusions in HSLA steel multipass weldments utilizing optical microscopy and examination and EDX analysis in a SEM. The results of the study suggest that the mean diameter of inclusions in the final pass of a GMAW weldment in a 2.0 inch HSLA-100 plate is larger than the mean diameter of those in the root pass. Additionally the inclusion material in the final pass contains a greater amount of Si and Ti deoxidation products than that in the root pass. The larger size, composition and complex structure of the inclusions in the final pass suggest that they contain deoxidation products from previous welding passes which have been released through remelting and coalesced into larger inclusions.

iii

TABLE OF CONTENTS

I. INTRODUCTION

The U.S. Navy's interest in reducing construction costs in its shipbuilding programs has resulted in research into the adoption of newly developed precipitation-hardened high strength low alloy (HSLA) steels. Commercially developed ASTM-A710 copper precipitate hardened steel in the 552-MPa yield range offers economical replacement for the currently utilized HY-80 steel of similar performance and has recently been certified for shipbuilding use. Certification of a similar 689-MPa yield HSLA-100 steel to replace HY-100 is expected soon.

One of the greatest advantages offered by these products is the cost savings involved in structural fabrication via welding processes (Anderson et al., 1987, p.21). HY steels require stringent preheat and interpass temperature control in order to meet weld strength specifications for shipbuilding. The extreme hydrogen sensitivity of the HY steels further limits their weldability. Use of the new HSLA steels permits welding under much less stringent heat input and temperature controls. ASTM-A710 was certified for use with the current low-hydrogen HY-80 welding consumables. Current efforts towards certification of HSLA-100 steel have utilized the HY-100 welding consumables. While use of already developed HY welding consumables has yielded adequate performance, research continues into the effect of using the HY materials for welding HSLA steels. Among the many factors influencing the development of sufficiently tough and strong welds in these steels, the distribution and composition of nonmetallic inclusions within the fusion zone has been shown to play a key role (Court, Pollard, 1985, p.427).

The focus of this study is an examination of the size, distribution and composition of non-metallic inclusions in HSLA-100 weldments produced with HY-100 consumables.

1

These weldments were supplied for study by the David Taylor Naval Ship Research and Development Center and are a product of that laboratory's ongoing research effort into the certification of HSLA-100 steel.

II. BACKGROUND

A. CHARACTERISTICS OF HSLA 100 STEEL

Development of a 689-MPA yield structural material has proceeded essentially as a follow on to the successful adoption of the ASTM-A710 commercial product. Clearly, these "HSLA" steels are not in fact true "low alloy" steels. In fact, the high copper (Cu) and nickel (Ni) content of these steels are expected to make the raw material for fabrication approximately 10% more expensive than the corresponding HY steels (Miglin, 1986, p.3). HY steels develop their strength from conventional quench and temper heat treatments. The HSLA steels attain similar performance through alternate strengthening mechanisms including precipitation and dispersion strengthening, grain refinement, solid solution strengthening and mechanical processing (Natishan, 1989, pp.5-22). All but the last are achieved through alloy additions.

HSLA-100 (and ASTM-A710 from which it is derived) owe much of their strength properties to the precipitation strengthening mechanism. Goodman, Brenner and Low (Goodman et al., 1973) investigated the precipitation of copper from a supersaturated iron-copper (Fe-Cu) alloy. Aging of such a supersaturated Fe-Cu alloy (See Fig. 1) results in precipitation of coherent body centered cubic non-equilibrium copper rich clusters. Peak hardness is achieved during the precipitation of this coherent non-equilibrium phase. Overaging results in the transformation and growth of these precipitates to larger equilibrium phase epsilon-copper particles. The best combination of toughness and strength is achieved in the overaged condition (Cox and Coldren, 1986,p.6).

3
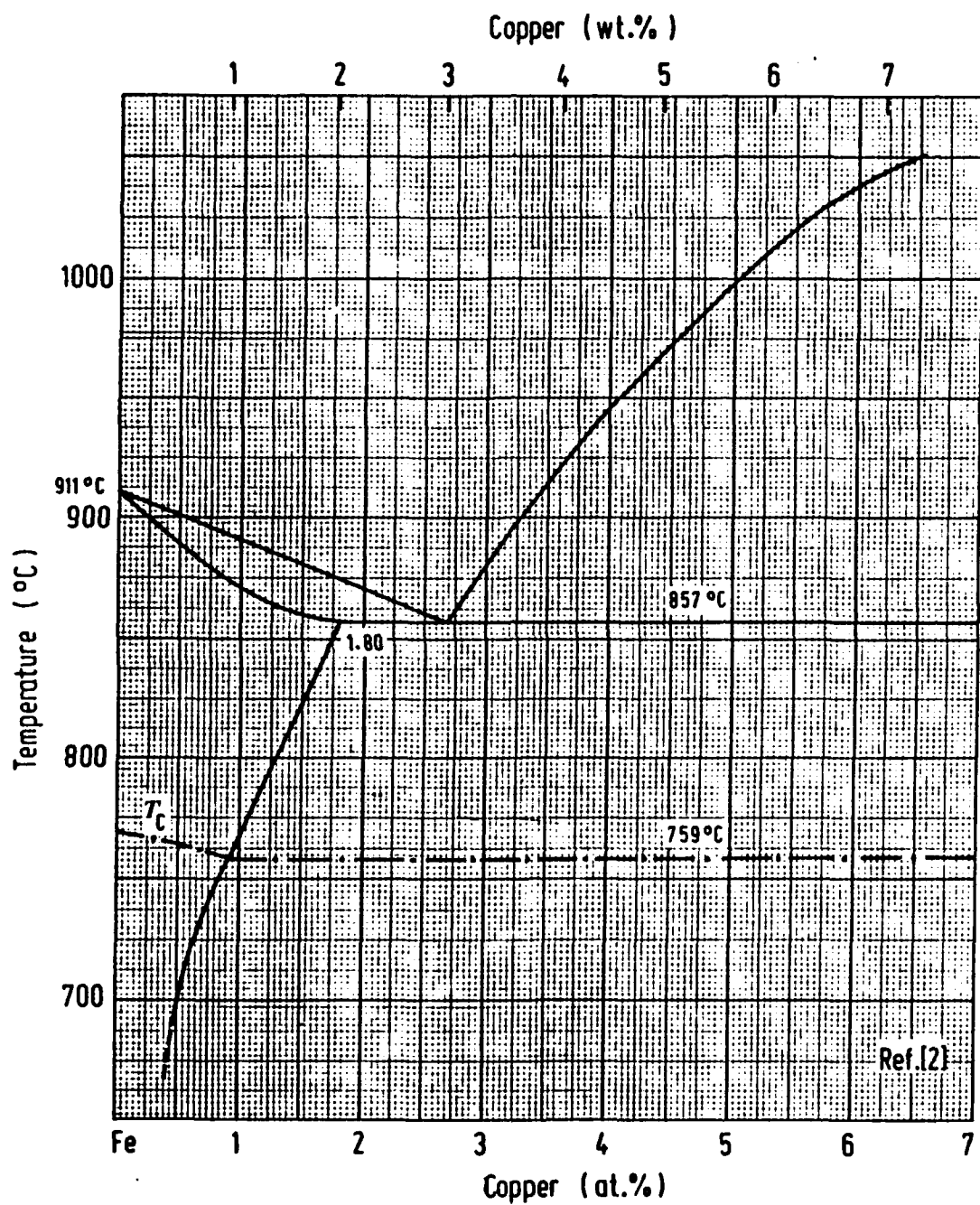
Figure 1
Phase diagram Fe-Cu system (Kubaschewski, 1982, p.37).

4

In addition to its precipitation strengthening effect, copper also increases the corrosion resistance of alloyed steels and decreases susceptibility to hydrogen induced cracking (HIC) (LeMay et al., 1984, p.65).

The low carbon (C) content contributes to good weldability, lowers the susceptibility to hydrogen (H) embrittlement and also results in decreased notch sensitivity (greater Charpy Vee Notch (CVN) toughness) and ductile to brittle transition temperature (DBTT) (Natishan, 1989, p.2). Niobium (Nb) additions form carbonitride precipitates during hot rolling which pin austenite grain boundaries, inhibiting grain growth and resulting in a finer transformed ferrite grain size. This effect occurs at very low niobium concentrations, permitting grain size refinement, and corresponding improvements in toughness, by microalloying with no increase in DBTT. In addition to the beneficial effects of grain refinement, the tendency of niobium to form very fine insoluble carbonitride precipitates results in a dispersion strengthening effect. Finally, very small quantities of niobium act as an austenite stabilizer (Natishan, 1989, p.28).

Nickel (Ni) additions contribute to strength and toughness by solid solution strengthening while actually lowering the DBTT. Nickel prevents the hot shortness phenomenon often observed in copper-bearing steels. Nickel is also an austenite stabilizer. By lowering the temperature at which austenite transforms to ferrite, greater strength can be achieved in mechanical processing (austenite grain conditioning) as well as limiting ferrite grain growth (Potkay, 1987, p.16).

Other alloy components including manganese (Mn) and aluminum (Al) may be added to remove or react with otherwise harmful contaminants such as sulfur (S) and oxygen (O). The addition of manganese for example prevents the formation of harmful FeS at grain boundaries by reacting with dissolved sulfur to form MnS. MnS inclusions

5

become extremely deformed during the controlled rolling process associated with structural steels. Rare earth additions may be made in processing to control the shape of these inclusions. More brittle oxides tend to break up during the rolling process and are also undesirable. The effects and consequences of inclusion distribution and base metal alloy composition on the welding of these materials will be discussed at greater length in following sections.
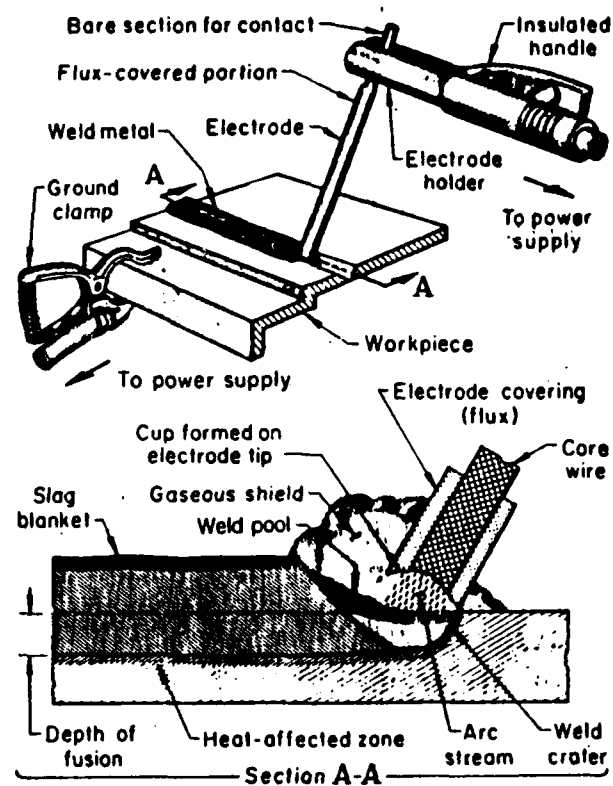
The combined effects of the microalloying components and the low carbon content of the HSLA-80/100 steels would indicate a very favorable weldability which has in fact been realized in research thus far.

B. WELDING PROCESSES

As previously mentioned, all developmental work on welding of HSLA steels has been conducted using welding consumables developed for HY-80/100 structural steels. The use of these welding consumables results in some restriction of welding process variables (preheat, energy input, interpass temperature limits, etc...) which are a result of limitations of the filler metal and not the base material (Potkay, 1987, p.32). The general characteristics of the most common arc welding processes used in fabrication with HSLA steels are described briefly below.

1. Shielded Metal Arc Welding (SMAW)

Shielded metal arc welding (See Fig. 2) utilizes an electrode which is composed of the desired filler metal covered with a decomposing flux sheath. An arc is maintained between the tip of the filler metal electrode and the base metal. The arc provides energy to melt both the base metal and the filler metal welding electrode. SMAW is usually conducted with a direct current straight polarity (DCSP) or AC

6

Bare section for contact

Insulated handle

Flux-covered portion

Weld metal

Electrode

Electrode holder

Ground clamp

A

To power supply

Workpiece

To power supply

Electrode covering (flux)

Cup formed on electrode tip

Core wire

Slag blanket

Gaseous shield

Weld pool

Depth of fusion

Heat-affected zone

Arc stream

Weld crater

Section A-A

Figure 2
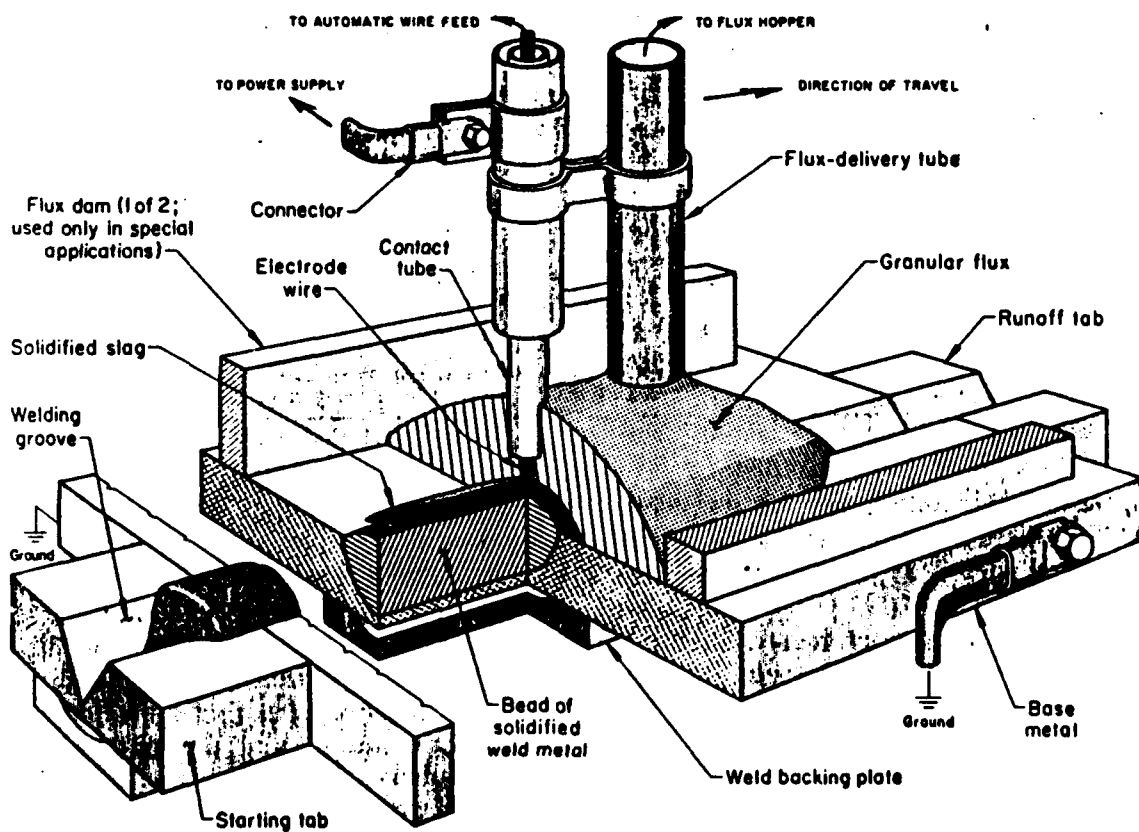SMAW process (Metals Handbook, 1983, p.76).

7

electrode. The chief advantage of SMAW is the small size, simplicity and low cost of the equipment. Disadvantages revolve around relatively low deposition rates and poor weld metal protection afforded by the flux sheath. Relatively low welding currents must be used and the discontinuous (due to the length of the electrodes) process must be carried out manually.

2.   Submerged Arc Welding (SAW)

Submerged arc welding (See Fig. 3) utilizes a continuous filler metal wire electrode. A separate granular flux material is fed into the weld ahead of the welding arc between electrode and base material. Direct current reverse polarity (DCRP) is normally used in SAW. AC may be used to minimize "arc blow" when extremely high currents are used. Advantages of SAW include good protection of the weld by the molten slag blanket, a high deposition rate and the ability to use high welding currents. The continuous filler wire electrode allows the process to be automated. Unfortunately the physical nature of the welding equipment is fairly restrictive in terms of the layup of the base materials. Overhead SAW, for example, is impractical. The high heat inputs and blanketing action of the slag can result in coarse grain formation in the fusion zone.

3.   Gas Metal Arc Welding (GMAW)

Gas metal arc welding (See Fig. 4) also utilizes a continuous consumable filler metal electrode. In this process the arc maintained between the electrode and base metal again melts both to allow a fusion weld to form. DCRP is normally used in GMAW. The molten weld pool is protected by an inert gas shield which is normally argon, helium or mixtures of both and other gases.

Figure 3
SAW process (Metals Handbook, 1983, p.114).
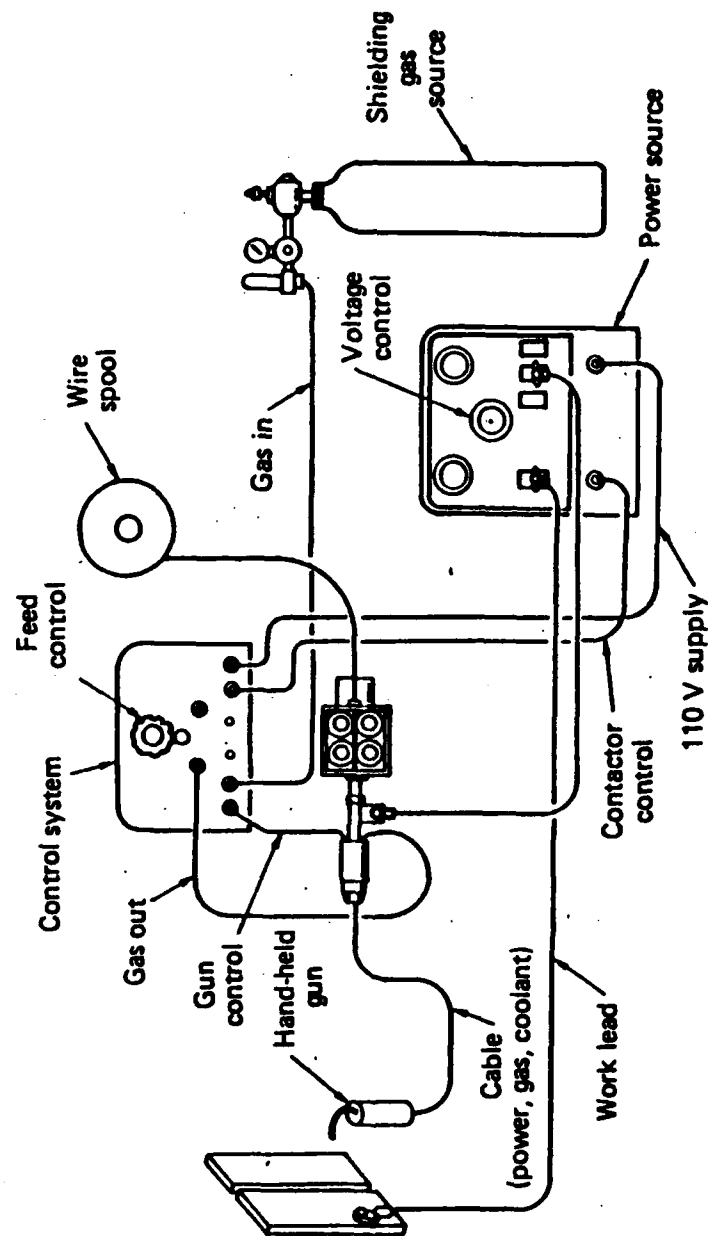
Figure 4
GMAW process (Metals Handbook, 1983, p.155).

10

4. Fluxes

SMAW and SAW both use a flux material which is melted by the heat of the arc to a glassy slag material. Welding of HY steels demands the use of special "low hydrogen" flux material. Low hydrogen SMAW electrode flux contains $CaCO_3$ which decomposes to produce a CO_2 atmosphere to protect the weld metal, much like that provided by the inert atmosphere in GMAW. Other materials, whose significance will be discussed later, are also added as binders, cleansing and alloying agents.

C. METALLURGY OF WELDING

When joining structural steels by fusion welding, it is desirable to achieve a weld metal deposit with high strength and good notch toughness. The strength and toughness of the weld are of course reflections of both the microstructure and chemical composition of the solidified material within the fusion zone. Studies involving the distribution and composition of nonmetallic inclusions within the fusion zone have thus concentrated on the relationship between these inclusions and the microstructure and chemical composition of the weld material. Nonmetallic inclusions are at the same time essential for, and harmful to, the production of a strong and tough material in the fusion zone.

1. Sources of Inclusions

Sources for primary and secondary non-metallic inclusions include slag-metal interaction, metal arc-atmosphere interaction, and interactions between molten filler and base metal. Inclusions may also appear from exogenous sources (Kiessling, Lange, 1980, p.101). The slag-metal interaction is that interaction between components of the molten flux and the weld pool. "Low-hydrogen" electrode fluxes for SMAW and SAW are high basicity index mixtures containing deoxidizers, alloying elements, slag producers, sources

11

of nonreactive gas for the arc atmosphere, binders and arc stabilizers. These compounds or their constituents in turn have some solubility in the molten metal of the weld pool. The solubility or the rate of precipitation of insoluble inclusions are functions of temperature and the agitation within the weld pool (Grong et al., 1986, p.1806). The extremely high temperatures achieved and the large surface area of the molten metal droplets combine to result in a highly reactive region within the arc between molten metal and arc atmosphere, especially near the electrode tip (Kuo, 1987, pp.61-62).

Melting of the base metal and agitation within the weld pool results in dilution of filler with base material within the fusion zone. Impurities within the base material can react with alloying elements in the filler, perhaps forming inclusions of undesirable shape, or depleting elements critical to development of a microstructure of desired morphology (Reeve, 1952, p.63).

Exogenous inclusions are those produced during the welding process, but exclusive of reactions involving the molten weld pool. Examples include tungsten inclusions from melting of the electrode in Gas Tungsten Arc Welding GTAW. Exogenous inclusions are nearly always harmful and hence undesirable.

2. Composition of Inclusion Types

While the inclusions present in the solidifying weld pool are similar to those present during the steelmaking process, the dynamics of their production, composition and distribution are in fact much more complex. The rapid cooling rates and relatively short reaction times occurring in the liquid weld pool result in the reaction processes being nonequilibrium in nature. Attempts to apply the equilibrium thermodynamic approach used in conventional steelmaking have hence proved relatively unsuccessful (Chai, Eagar, 1981, p.539). The following discussion will review recent research into the sources,

formation and effects of the various types of nonmetallic inclusions found in weld metal and HSLA welds in particular.

In conventional steelmaking practice, the content of undesirable dissolved elements such as oxygen, sulfur, and nitrogen can be approximated by chemical equilibrium considerations. For example, extremely dilute solutions of diatomic gasses such as nitrogen and oxygen in iron obey a simple relation known as Sievert's Law (Kuo, 1987, p.64). For oxygen this is expressed as follows.

$$K = [O]/P_{O_2}^{1/2} \qquad (1)$$

K = equilibrium constant

[O] = atomic oxygen concentration in solution

P_{O_2} = partial pressure of oxygen

The equilibrium constant K is related to the Gibbs Free Energy (G).

$$G = -RT\ln K \qquad (2)$$

R = universal gas constant

T = system temperature

Where deoxidizing elements such as aluminum, manganese, or silicon (Si) are added, further equilibria are established between the oxide products and dissolved oxygen. Unfortunately, such calculations assume the establishment of an equilibrium reaction temperature in a homogeneous solution. The conditions in the solidifying weld pool (particularly the cooling rate and the rate of advance of the solidification front) do not allow equilibrium to be established. A common solution for this problem in attempts to apply equilibrium thermodynamics to the welding process is the calculation of an effective reaction temperature based on analysis of the weld metal. An "after the fact" approach is of course useful in identifying the nature of inclusions of known atomic

percent composition. Even this analysis is affected by the formation of nonequilibrium complex inclusions of many phases. Attempts to establish an equilibrium correlation between slag material and dissolved oxides have also been unsuccessful. It appears that while free energy considerations can establish the direction of the reaction, the nonequilibrium nature of the reaction products prevents reliable prediction of concentrations of dissolved impurities or the consistency of precipitated inclusions from equilibrium phase diagrams (Dowling et al., 1986, p.1617).

a. Oxides

Deoxidation of the molten steel weld metal is of great importance in all welding processes (See Fig. 5). Oxygen content takes two forms, dissolved oxygen and oxygen precipitated in oxide inclusions. Sources of oxygen are the slag metal interaction and metal arc-atmosphere interaction. Elements such as aluminum and silicon are added to react with the dissolved oxygen and form less harmful oxide inclusion or to be separated out as slag. Flux mixtures in the SAW process containing varying quantities of CaF_2, Al_2O_3, CaO, MgO, SiO_2, TiO_2 and $CaCO_3$ were studied with respect to the effect of varying flux composition on overall oxygen content. One of the conclusions of this study was that the flux and hence slag compositions used did not greatly effect the oxygen content of the completed weld, unless $CaCO_3$ was used. The main source of oxygen was determined to be not the slag metal interaction but the metal arc-atmosphere interaction (North et al., 1978, p.66s). That is, the reaction of the hot metal droplets melted from the filler wire with the CO_2 produced by decomposition of $CaCO_3$ at the electrode tip. In fused fluxes not containing $CaCO_3$, the decomposition of other oxides within the arc was likewise determined to be the source of oxygen. In GMAW processes oxygen or carbon dioxide may be added to the gas mixture as an arc stabilizer

14
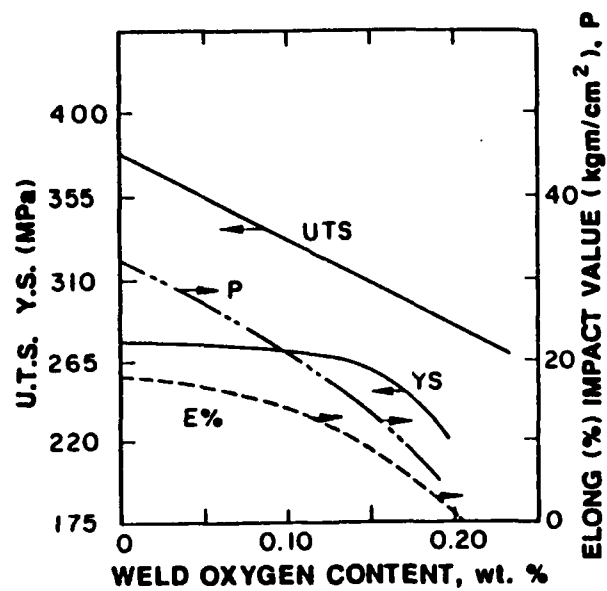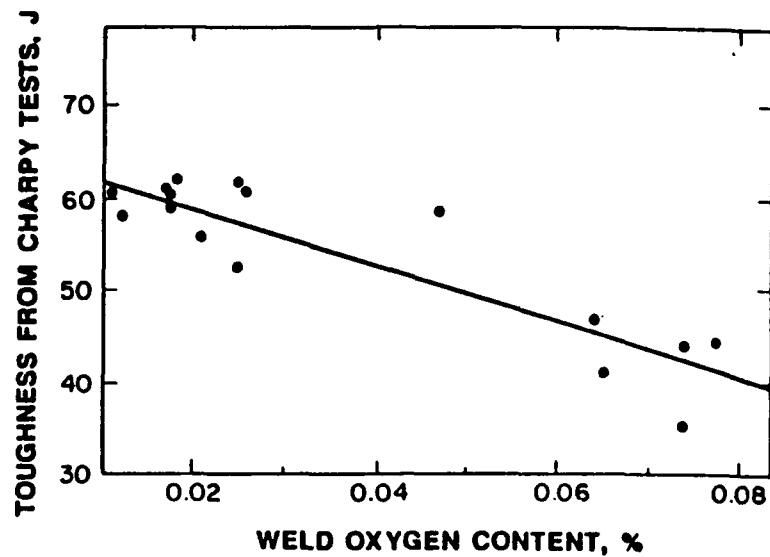
Figure 5
Oxygen content vs CVN energy in Nb microalloyed steel weld metal (Kuo, 1987, pp.70-82).

15

and hence result in the presence of atomic oxygen at the electrode tip. While it was determined that no conclusions with regard to oxygen content could be made based on equilibrium of the metal and slag, the study did uncover some discrepancies in earlier determinations of oxygen content by inclusion counting methods. The size of this discrepancy was incompatible with the limits of dissolved oxygen (North et al., 1978, p.69s). One is left to conclude that the remaining oxygen was contained in inclusions too small to be identified by optical counting methods. Another study attempted to relate the oxygen content of welds to the Mn-Si content of the flux additions. An empirical correlation was derived in this study. More interesting were results concerning inclusion size. In commercial steelmaking practice, a high Mn:Si ratio contributes to rapid growth of oxide and silicate inclusions in steel melts and hence better flotation as slag. The large size of the inclusions results in significant separation due to flotation predicted by Stokes Law (this phenomenon will be discussed in greater detail with respect to the distribution and size of trapped inclusions). Increases in the Mn:Si ratio also results in an overall increase in the size of trapped oxide inclusions. In the weld metals examined, the high Mn:Si ratio, while reducing overall oxygen content, contributed to a significant reduction in size of trapped oxide and silicate inclusions (Grong et al., 1986, p.1802). This correlates with the previous discussion of the oxygen content in inclusions not identified by optical microscopy.

b. Nitrides

The presence of nitride inclusions in weld metal is generally an indication of improper shielding of a shielded arc process weld resulting in a reaction with atmospheric nitrogen. Nitrogen tends to combine with many otherwise desireable alloying

16

elements to form extremely undesirable nitride inclusions. Such inclusions often have a polygonal or needle-like structure, and are good crack initiators (Kuo, 1987, p.64).

c. *Sulphides*

Dissolved sulphur and sulphide inclusions can be significant, especially in filler metal highly diluted by molten base metal. The dissolved sulphur can combine preferentially with important deoxidizers, such as manganese, and result in a depletion of these elements, or an upset of the Mn:Si ratio. MnS inclusions within the HAZ have been shown to contribute to the hot-tearing phenomenon in welded steels (Kiessling, Lange, 1980, p.101). Investigations into sulphide inclusions within the fusion zone have recently yielded interesting results from extremely precise X-ray mapping of the inclusions. Some globular MnS inclusions are observed often apparently nucleated by smaller insoluble oxide inclusions. Researchers have also identified Cu_2S inclusions within the fusion zone of HSLA-80 steel welds. The source of copper in these inclusions is presumably the dilution of the filler metal by the copper rich base metal. Such inclusions appear to take the form of Cu_2S envelopes containing oxide or silicate inclusions (Court, Pollard, 1985, p.429). Some believe that only certain types of inclusions (oxides) are effective in nucleating a desirable microstructure within the solidifying weld pool. Sulphides which envelope these oxide inclusions tend to form larger inclusions and reduce the distribution of desirable oxide nucleation sites. The resulting Cu_2S envelopes are not believed to be favorable for the development of this microstructure (Dowling et al., 1986, p.1611).

3. Size and Distribution of Inclusions

Stokes Law can be used to predict the average velocity of precipitate particles in a liquid pool. Calculations of this sort yield some limiting value on the size of

trapped inclusions in steelmaking. Until recently there was little data to indicate whether such a relation applied to the elimination of inclusions in a molten weld pool by flotation. Using values for normal inclusions found in weld metal indicates that this is indeed not the case. The following mathematical expression of Stokes Law is that commonly encountered in steelmaking.

$$v = (Gdk)/(18n) \qquad (3)$$

G = gravitational constant

d = particle diameter

p = density difference between liquid metal and inclusion

n = viscosity of liquid steel

The value of $(Gk/18n)$ in equation (3) is generally known as the Stokes parameter. In the case of manganese silicate inclusions in liquid steel, the Stokes parameter has a representative value of 0.6 micron sec. The average velocity of such inclusions of average diameter of 2 microns is on the order of 3 microns/sec. Utilizing the above development and the fact that fluid velocities due to turbulence in the weld pool are several orders of magnitude greater than the predicted flotation velocity, Grong (Grong et al., 1986, p.1806) has proposed a mechanism which appears to explain the dominance of very fine inclusions found in weld metal. It appears that the molten weld pool material is divided into two zones (See Fig. 6). In the inner "hot" zone, the turbulent flow fields of the molten weld pool dominate the growth and movement of the inclusions. The turbulent nature of this region results in good growth and separation of the oxide inclusions. The beneficial effects of agitation on the growth of the inclusions, and the turbulent flow in the weld pool tend to drive the inclusions to the surface. Once these inclusions reach the surface, they tend to remain there due to surface
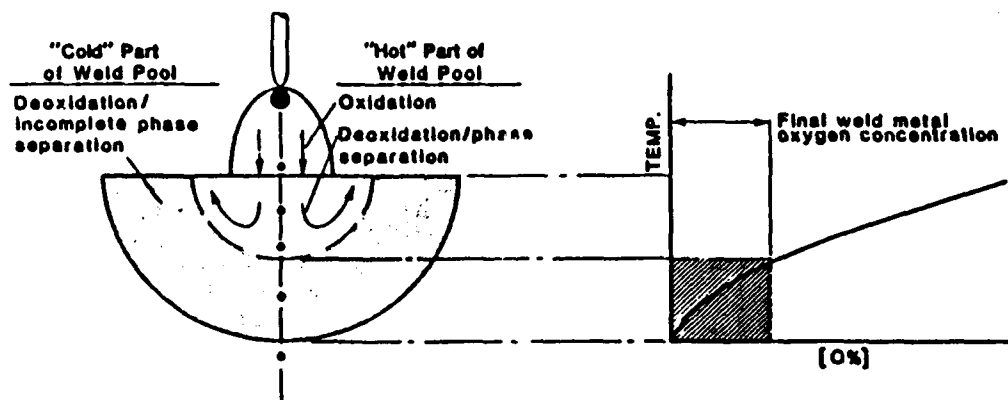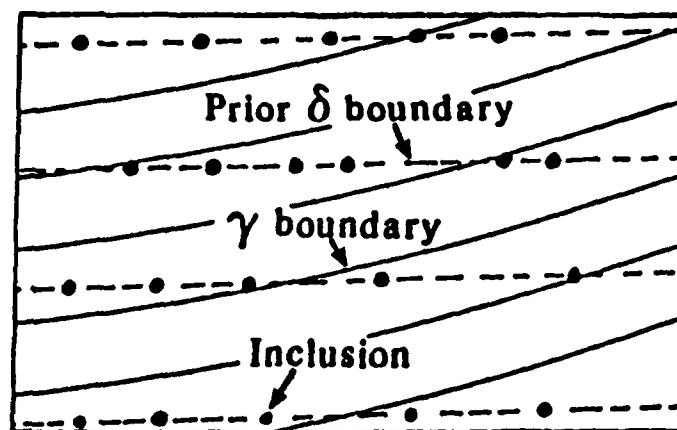
Figure 6
Zones in the weld pool (Grong et al., 1986, p.1799).

energy considerations. In the cooler, less turbulent outer zone, nucleation exceeds growth and the small precipitates cannot float to the surface. The very fine precipitates are thus trapped in the weld pool. This hypothesis is supported by the experimental evidence as the trapped inclusions are primarily extremely fine precipitates. Since the turbulence of the weld pool is determined to a great extent by the welding parameters (voltage, current, welding speed etc...) variation of these parameters alone should have a significant effect on the inclusion size and distribution.

Models concerned with predicting the effects of inclusions on microstructure development within a weld normally assume a uniform distribution of inclusions throughout the fusion zone. Studies of the solidification process indicate that this may not be entirely true. It is thought that as the solidification front moves through the freezing weld metal, it "pushes" larger inclusions ahead of it. These large inclusions are then trapped at the grain intersections of the cellular solidification front characteristic of this solidification process (See Fig. 7). These large inclusions are then trapped preferentially along the boundaries of the grains where they may effect the final microstructure in two distinctly different mechanisms. If the weld metal solidifies as austenite, these large inclusions will be trapped along grain boundaries and hasten the nucleation of allotriomorphic grain boundary ferrite which is undesirable in the final weld microstructure. If the metal solidifies as delta ferrite, the preferential concentration of inclusions at grain boundaries will actually be advantageous since the same inclusions will then be trapped internal to the transformed austenite grains and will be able to nucleate desirable acicular ferrite (See Fig. 8). Finer precipitates are trapped immediately within the solidification front and are thus not similarly affected. Scanning electron

20
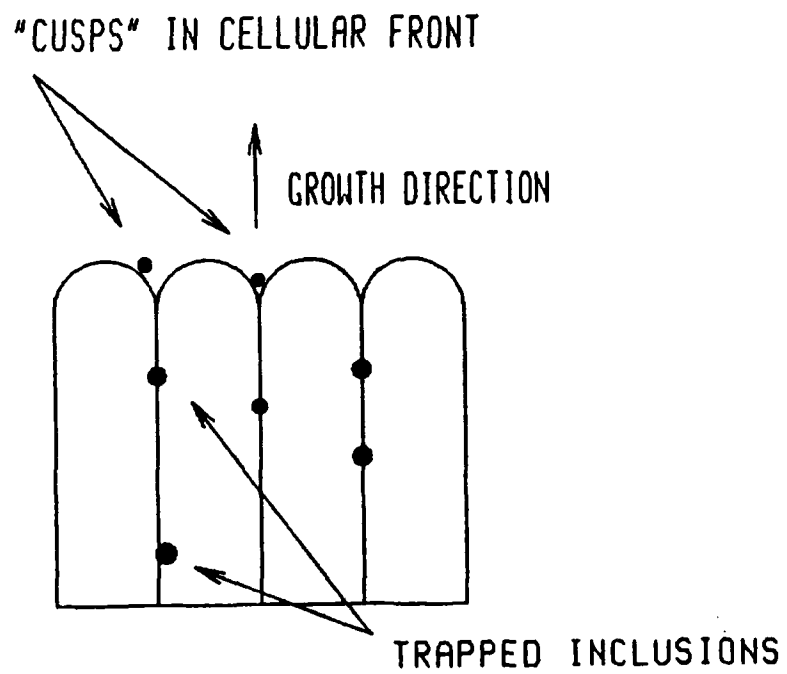
Figure 7
"Trapping" of inclusions within the solidifying weld pool.
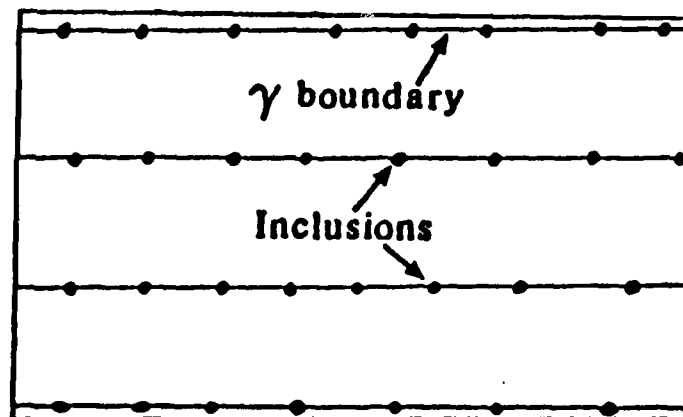
Figure 8
Effect of inclusions on microstructure (Bhadeshia, 1988, p.670).

microscopy of weld metals has identified such a nonuniform distribution of oxide inclusions in HSLA welds (Bhadeshia, Sugden, 1988).

4. Role of Inclusions in the Nucleation of Acicular Ferrite

Inclusions in weld metal are generally undesirable due primarily to their adverse effect on notch toughness (especially in the case of oxides and nitrides) and the depletion of deoxidizers and hot tearing in the case of sulphide formation. Inclusions also play a vital role in the nucleation of a very desirable microconstituent, namely acicular ferrite. Acicular ferrite consists of intragranularly nucleated fine Widmanstatten ferrite needles. These ferrite needles form an interlocking structure which is very resistant to crack propagation. Evidence conclusively indicates the correlation between increased CVN toughness and volume fraction of acicular ferrite in low alloy steel welds (Matlock, Edwards, 1986, p.7; Kuo, 1987, p.189; See Fig. 9). The question then becomes; How do we maximize the final volume fraction of acicular ferrite in the weld metal microstructure?

Inclusions appear to play a key role in the nucleation of intragranular Widmanstatten ferrite plates. Some researchers have proposed a direct correspondence between the oxygen content of the weld metal and the percent of acicular ferrite in the weld microstructure. Superficially, the experimental evidence seems to confirm this early postulate. Optimum oxygen content for SAW welds was determined to be between 200 and 260 ppm (Harrison, Farrar, 1981). Theoretically this concentration provided optimum size and distribution of oxide inclusions for nucleation of acicular ferrite. Higher oxygen concentrations resulted in a greater volume fraction of finer precipitates which inhibited austenite grain growth and preferentially nucleated grain boundary allotriomorphic ferrite. Lower concentrations of oxygen resulted in a weld metal microstructure consisting

23
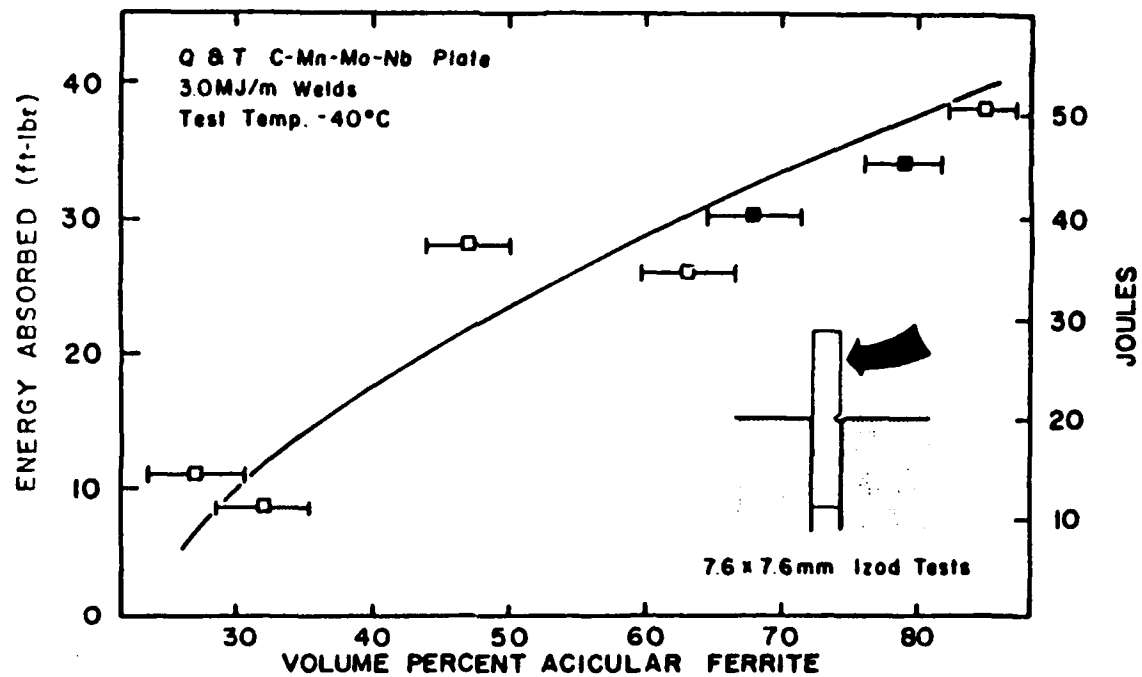
Figure 9
%Acicular ferrite vs CVN energy in Nb microalloyed steel weld (Kuo, 1987, p.189).

24

primarily of parallel lath ferrite. This microstructural change was attributed to the reduced number of nucleation sites for intragranular nucleation. More recently is has been noted that the previous research neglected the effects of alloy component depletions at greater oxygen levels, especially manganese. The greater fraction of acicular ferrite at certain oxygen concentrations was attributed mainly to hardenability considerations while virtually no correlation with oxide or inclusion content in general was observed (Bhatti et al., 1984, p.226s).

Somewhere between these two extremes lie theories suggesting that conditions favorable for nucleation of acicular ferrite consist of both the proper size and distribution of inclusions which favors heterogeneous nucleation of the Widmanstatten structure and the proper alloy concentration resulting in favorable hardenability. The weight of literature reviewed suggested that conditions favorable for nucleation of acicular ferrite must include a distribution of inclusion material larger than 0.5 microns within the austenite grains and the suppression of the austenite-alpha ferrite transformation temperature by some mechanism. At high transformation temperatures, the nucleation of grain boundary ferrite will be energetically preferred over heterogeneous nucleation of intragranular ferrite. As the transformation temperature is lowered, heterogenous nucleation becomes favored (Ricks et al., 1982, pp.738-739). Generally, dissolved oxygen and oxide inclusions provide both these conditions and hence were associated with acicular ferrite formation in earlier studies. Of course other alloy additions may serve a similar purpose and hence also have an impact on the final volume fraction of acicular ferrite in the weld metal. Alloying of the filler metal by molten base metal may similarly effect the final weld microstructure. The number of variables involved in the welding process can make it difficult to isolate a single mechanism responsible for the

25

final microstructure of the weld. An example is research which indicates less acicular ferrite in welds on calcium (Ca) treated HSLA steels that on calcium-free steels of the same composition. No calcium-containing inclusions are usually identified in the fusion zone of any welding process. The mechanism at work here is not understood (Bhatti et al., 1984).

If one accepts the link between inclusion content and acicular ferrite content, the next question involves what types of inclusions are more favorable for this particular heterogeneous nucleation process. Earlier observations characterized some inclusion types, especially sulphides or inclusions covered in sulphide envelopes, as noncontributors to acicular ferrite nucleation. As with the earlier observations involving oxygen content, recent observations taking other variables into account have established no correlation between an inclusion's phase or composition and its ability to nucleate acicular ferrite (Dowling et al., 1986, p.1622).

5. **Summary of Current Research**

The Navy's interest in ship construction applications of HSLA steels has resulted in a flurry of experimental and theoretical research into all aspects of welding such materials, including the effects of non-metallic inclusions in the welding process.

Ricks, Howell and Barrite (Ricks et al., 1982) have studied the microstructure of HSLA steel weld metals in detail. They were particularly interested in conditions preferential to the formation of acicular ferrite. In their observations of low carbon weld metal beads on HSLA plate they found that multiple plates of intragranular Widmanstatten ferrite were associated with non-metallic inclusions trapped within prior austenite grains. They concluded that the primary nucleation sites for acicular ferrite were refractory inclusions. The authors indicated that nucleation of ferrite will be

energetically favored, first at austenite grain boundaries and then at any inclusions, over homogeneous nucleation. Oxides, sulphides and silicate inclusions were all observed within the weld metal. No indication of preferential nucleation by any one type of inclusion was observed, nor apparently any segregation of inclusion type or size. The authors also conclude that since nucleation of grain boundary ferrite is a process which competes with the heterogeneous nucleation of acicular ferrite, the distribution or mean size of inclusions may also play a role in the development of the desired microstructure.

Harrison and Farrar (Harrison, Farrar, 1981) studied the formation of acicular ferrite in HSLA welds as a function of the oxygen content of the weld metal. The effects on microstructure of a variation of oxygen content from 600 ppm to 60 ppm in SAW weldments were observed. The experimental procedure was designed to hold the concentrations of all other elements constant. The authors found that high oxygen content (600 ppm) welds contained very little acicular ferrite. At 300 ppm, the microstructure was primarily acicular ferrite. When the oxygen content was further reduced to 58 ppm, the percentage of acicular ferrite in the microstructure was also reduced. Apparently the number of oxide inclusions at an oxygen concentration of 58 ppm was insufficient to sustain the nucleation of acicular ferrite over that of grain boundary ferrite. The increase in acicular ferrite with the reduction from 600 ppm to 300 ppm is explained by a depression of the austenite to ferrite transformation temperature. While the authors did observe a change in oxide inclusion size with the change in oxygen concentration, no relationship between oxide particle size and the final microstructure was advanced.

Dowling, Corbett and Kerr (Dowling et al., 1986) attempted to determine if any correlation exists between inclusion composition and the nucleation of acicular ferrite in HSLA weldments. Submerged arc welds were deposited on an HSLA steel base plate

27

with various fluxes and metallic additions to the flux. The researchers observed an average inclusion size of between 0.4 microns and 0.6 microns. This size was unaffected by variations in flux composition including the addition of powerful deoxidants such as aluminum and titanium. Inclusions observed included Al_2O_3-MnO-SiO_2 phases, MnS, TiO_2, Cu_2S, and others. Many inclusions were of a multi-phase complex character. No correlation between inclusion type or geometry and percent acicular ferrite in the final microstructure was found in this study. The authors suggest that since Al_2O_3-MnO (galaxite) inclusions were present in all samples in similar size and distribution, this inclusion could be responsible for the large proportion of acicular ferrite also found in all samples. Court and Pollard (Court, Pollard, 1985) conducted a similar study of SMAW weldments on HSLA steels. The inclusion size and composition observed were similar to the data obtained from the SAW weldments.

The study of Bhadeshia and Sugden (Bhadeshia, Sugden, 1988) into the distribution of inclusions within HSLA weld deposits was mentioned earlier. They have developed a model which predicts a nonuniform distribution of inclusions within solidifying weldments. This research indicates that inclusions in the 1 micron to 3 micron size range do in fact exhibit a nonuniform distribution within the final microstructure of their samples of low and medium carbon filler material on HSLA plates. The alignment of the inclusions suggests that they were trapped along delta ferrite grain boundaries as the weld pool initially solidified. The authors indicate that these inclusions then served as nucleation sites for intragranular ferrite, contributing to the high percentage of acicular ferrite in the final microstructure. The size of the inclusions observed in this study is of particular interest. The inclusions in the welds examined (presumably GMAW) ranged in size from 1 micron to 3 microns. This is somewhat

28

larger than that reported by other researchers using similar processes and materials. Smaller inclusions were not affected by the moving solidification front and thus remained randomly (uniformly?) distributed. However, when the larger inclusions became segregated at austenite grain boundaries, the amount of acicular ferrite in the weldments dropped sharply. This indicates that only the larger inclusions served as nucleation sites for acicular ferrite while the smaller ones, whose distribution remained constant, did not.

The overall conclusions reached from the literature reviewed are summarized in the following two statements.

1) Inclusion compositions in welds will be determined primarily by the composition of the filler metal and flux or shielding gas. The inclusions will in many cases be multiphase and will be of nonequilibrium composition. The size and distribution of the inclusions will also be strongly, if not completely, determined by the welding process and parameters selected.

2) Inclusions play an essential role in the nucleation of the desirable microconstituent acicular ferrite within the solidifying weld metal. The proper intragranular distribution and average size of these inclusions is critical but not their composition. Equally important to the inclusion content, and in many cases related to it, is a chemical composition which results in an austenite to alpha ferrite transformation temperature at which heterogeneous nucleation of intragranular Widmanstatten ferrite is energetically preferred to nucleation of ferrite at the austenite grain boundaries.

III. CURRENT WORK

A. PURPOSE

The David Taylor Naval Ship Research and Development Center is currently involved in a research and development program aimed at certifying the HSLA-100 steel (developed as a follow on to the ASTM A710 HSLA-80 steel) for shipbuilding. As a part of this program, the certification of welding consumables compatible with the new steel has also been carried out. As in the HSLA-80 program, the welding consumables used for HY steel have been used and found to achieve required strength and toughness requirements in the new steel. The use of these HY-100 consumables results in some restrictions in the welding processes due to the filler material.

The purpose of this project is to examine HSLA-100 weldments (deposited with HY-100 consumables) with respect to the size, distribution and composition of nonmetallic inclusions within the fusion zone. Information regarding the size and distribution of inclusions will be gathered primarily by means of optical microscopy while information about the composition and distribution of phases within inclusions will be gathered by use of a scanning electron microscope and energy dispersive X-ray analysis (EDX).

As an important adjunct to this project, an identical analysis was conducted on a sample steel for which information on inclusion content and distribution was readily available. This effort allowed development of an experimental technique suitable for very small samples particularly with respect to accurate visual counting and analysis of multiphase complex inclusions utilizing EDX analysis. The importance of the

30

development of a standard technique will be discussed in greater detail in the sections dealing with that particular portion of the analysis.

## B.   EXPERIMENTAL PROCEDURE

The experimental procedure consisted of two distinct operations. Statistical and qualitative analysis of optical micrographs yielded information about the size and distribution of inclusions within the weld cross section. Qualitative visual analysis of images and micrographs from the scanning electron microscope and analysis of inclusions through EDX analysis yielded information about the composition of individual inclusions.

1.   Specimen Preparation

Specimen preparation was identical for both optical and electron microscope observation. General guidance for the preparation of metallographic specimens is given in ASTM Standards, Volume 3, Section E3 (ASTM Standards, pp.75-78). Specific treatment of samples will vary depending on the specimens physical and chemical characteristics. Therefore, the following discussion addresses only certain unique aspects or pitfalls encountered in the preparation of the samples used.

In order to greatly simplify the identification of any gross asymmetries or nonuniformities of distribution, composition, size or shape of inclusions, the samples were sectioned and mounted in order to isolate such characteristics as much as possible to a single sample. For example, the ASTM 9260 spring steel examined in the preliminary study was expected to exhibit an asymmetry (in terms of aspect ratio) of the deformable MnS inclusions due to rolling. Observation of this characteristic was greatly facilitated by observing sectioned planes parallel and perpendicular to the rolling axis (See Fig. 10). Observation of both samples allows a qualitative comparison of the effects of

31

ASTM 9260 TEST SAMPLE
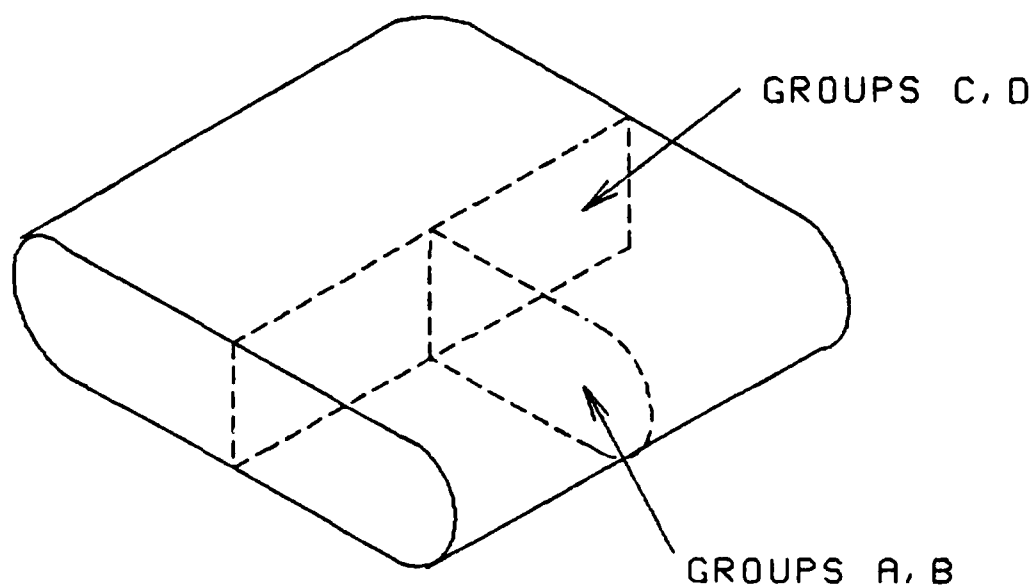
GROUPS A,B CUT PERPENDICULAR TO ROLLING AXIS
GROUPS C,D CUT PARALLEL TO ROLLING AXIS

Figure 10
Sectioning of ASTM 9260 sample (see text for details).

the processing on the MnS inclusions in this steel. Similarly, the weld samples were sectioned in order to emphasize any nonuniformity in inclusion size, composition or distribution between weld metal near the fusion boundary and that nearer the inner zone of the weld metal.

Samples prepared for optical microscopy must not be overpolished. Small scratches remaining in the surface are easily discerned from inclusions by the eye. Overpolishing can result in undesired removal of small inclusions (eg. oxides) and blurring and apparent enlargement of others. This is especially true in the case of extremely soft or deformable inclusions (eg. MnS) which may be removed faster than the surrounding matrix.

The sample should be cleaned extremely well between polishing media and at the conclusion of the final polishing. Retained polishing media can contaminate subsequent polishing operations, which is of course undesirable. Very fine polishing media (especially alumina) can also be retained in matrix inclusion boundaries or other surface irregularities and show up in EDX analysis. Cleaning in ethanol in an ultrasonic cleaning device was found most effective.

Specimens should be fine polished and observed immediately without etching. The purposed of this study was to gather information concerning the size and distribution of inclusion material within the bulk sample. Qualitative identification and measurement of the size of inclusions is easily carried out in the unetched condition. Etchants can be used to reveal the microstructure and the action of the inclusions in nucleating the final microstructure.

33

2. Optical Microscopy

A great diversity of "standard" methods exist for describing the inclusion content of steels. Most were developed for use in production steelmaking to describe the inclusion content of a particular steel product. They generally involve observing a large number of fields at a fixed magnification and comparing the inclusions observed with a standard chart, or counting intersections of inclusions with a standard grid overlayed on the fields. The ASTM Standards, Volume 3, Section E45 (ASTM Standards, pp.215-225) describes several standard procedures for determining inclusion content in steel samples through interpretation of numerous optical micrographs of the subject material. A variation of such a technique was used in the current study.

The next step in the experimental procedure was to obtain optical micrographs of the sections to be analyzed. The goal of this procedure is to obtain a statistically significant number of micrographs, representative of the size and distribution of inclusions within a specific part of the sample. Details concerning the procedures for actually obtaining micrographs can be found in the appropriate appendix (See Appendix A).

The sample was placed in the micrometer mount such that "strips" of photographs were obtained by simply advancing the micrometer along a single axis to obtain non-overlapping fields. (See Fig. 11) The result is a uniform distribution of fields across the desired section of the sample. Care should be taken to avoid "photographing inclusions" versus photographing the sample in order to analyze the inclusion distribution.

Fifty fields of each sample were obtained for the test run on the ASTM 9260 samples. From the results of this analysis it was determined that at least 100 fields per sample would be desirable for the weld samples.

FRAMES 1-25, GROUP A
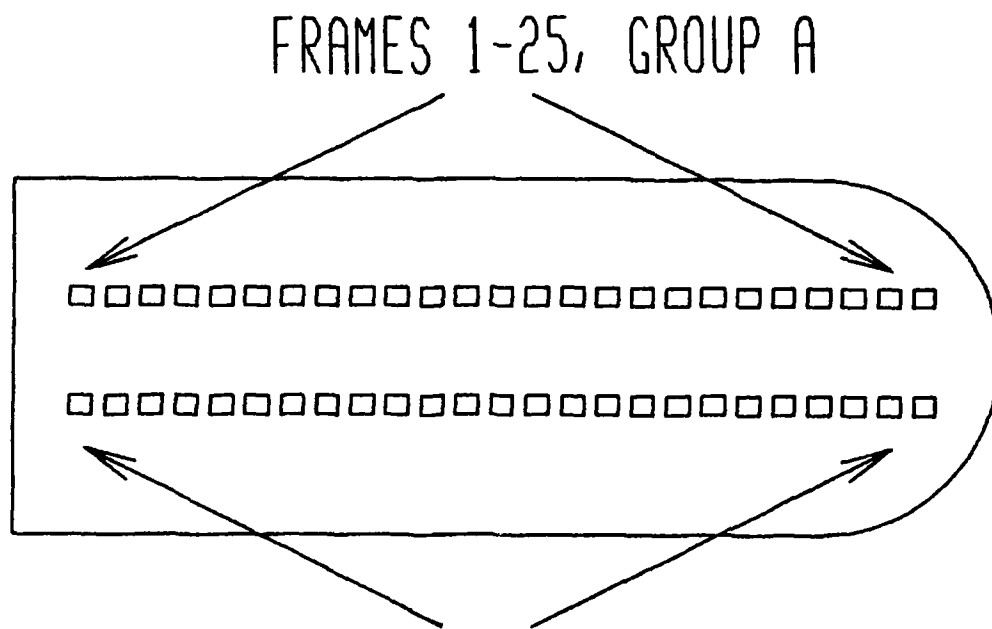
ASTM 9260 OPTICAL FIELD
ARRANGEMENT

FRAMES 1-25, GROUP B

Figure 11
Distribution of photographs in ASTM 9260 sample.

35

The micrographs obtained from this procedure were analyzed in order to determine the mean size of inclusions, area fraction of inclusion material, mean distance between inclusions and, in the case of the ASTM 9260 samples, the inclusion aspect ratio for each group of fields.

The following procedural steps were developed for reducing the photographic material to useful numeric data. A preliminary examination of all micrographs was made in order to identify approximately the largest inclusion in all fields. Analysis of the ASTM 9260 specimens resulted in a conservative useful lower limit of about 1.0 microns. This range of sizes was then broken down into equal segments. All micrographs were then examined and inclusions sorted by size into the various ranges. "Size" was determined in all cases by the measurement of maximum chord length across the inclusion. Statistical analysis could then be carried out on the resulting discrete data set. The aspect ratio was determined for the ASTM 9260 samples by dividing maximum by minimum chord lengths for non-spherical MnS inclusions. In this instance, the characteristic of interest was the difference in aspect ratio between the different groups of fields. In the weld samples, the characteristic of interest was the size and distribution of inclusions in each group of fields and the difference (if any) between groups of fields. Thus the mean size, area fraction and mean distance between inclusions were calculated. Sample analyses of portions of the data collected for the ASTM 9260 standard are contained in Appendix D.

3. Electron Microscopy

Information on the composition of inclusions was obtained by EDX analysis in a scanning electron microscope (SEM). A summary of the capabilities of the SEM is contained in Appendix B.

EDX/KEVEX analysis was carried out on the same samples as used in the optical microscopy portion of the study. For the ASTM 9260 test samples, analysis was performed first on inclusions of near the mean diameter, then on MnS inclusions and complex inclusions (MnS nucleated on other higher melting point inclusions). A similar approach was utilized for the weld samples. Analysis was performed on several inclusions of near mean size, then on any others of particular interest due to peculiarities in structure or composition. Details on the gathering and manipulation of EDX spectra via the KEVEX equipment and software is included in Appendix C.

EDX analysis yielded two types of data. Through elemental analysis of representative inclusions within each sample, it was hoped to identify any non-uniform distribution of inclusion type or phase. Analysis of individual inclusions through the use of equilibrium phase diagrams was also carried out in order to determine, if possible, phases present in complex inclusions. A description of such an analysis is included as an example in Appendix D.

IV. RESULTS AND DISCUSSION

A. HSLA WELDMENT SAMPLE

Material specifications for the HSLA-100 base material of the weldment examined are included in Table I. The material composition is typical of the HSLA copper precipitate hardened steels. The weldment examined was produced by the GMAW process utilizing HY-100 welding consumables. Summaries of the material specifications of the welding consumables and the welding process variables are included in Tables II and III, respectively.

Fundamental to the conduct of this analysis was the fact that the thickness of the material required a multipass technique for completion of the weld (See Fig.12). The method of sectioning was selected to simplify analysis and comparison of the highly diluted filler material in the root pass of the weld and the less diluted material near surface of the final weld pass (See Fig.13). Analysis of cross sections parallel to the longitudinal axis of the weld was conducted in order to insure that the area analyzed was of a nearly constant dilution. It was anticipated that any segregation (by size or composition) of inclusion material within individual passes would be obscured by remelting incurred by subsequent welding passes. Segregation of inclusions by composition, and perhaps size, was anticipated between the root pass and final pass due to the gradient of base metal dilution which is certainly present.

TABLE I

ELEMENT	X
C	.06
Mn	.75/1.05
Si	.40
P	.015
S	.006
Ni	3.35/3.65
Mo	.55/.65
Cr	.45/.75
Al	.02/.04
Cu	1.45/1.75

HSLA-100 base metal chemical composition.

TABLE II

ELEMENT	%
C	.12
Mn	1.50/2.00
Si	.30/.50
P	.010
S	.010
Ni	1.95/3.10
Mo	.40/1.00
Cr	.65/1.05
V	.04
Al	.04
Ti	.04
Cu	.16
Zr	.04

HY-100 GMAW electrode wire chemical composition.

TABLE III

BASE MATERIAL	HSLA-100, 2 INCH PLATE
JOINT DESIGN	DOUBLE VEE (SEE FIG.2)
FILLER	1/16 INCH DIAMETER M-128S WIRE (SEE TABLE 2)
PROCESS	GMAW SPRAY TRANSFER
SHIELDING GAS	98% ARGON, 2% OXYGEN
FLOW RATE	50 CFH
WELDING POSITION	FLAT
VOLTAGE	26 VOLTS
CURRENT	300 AMPERES
WELDING SPEED	8.5 INCHES/MIN
PREHEAT	60 F.
INTERPASS	225 F.
HEAT INPUT	55kJ/IN
PASSES	36

GMAW welding process variables.

41

WELD BEAD SEQUENCE
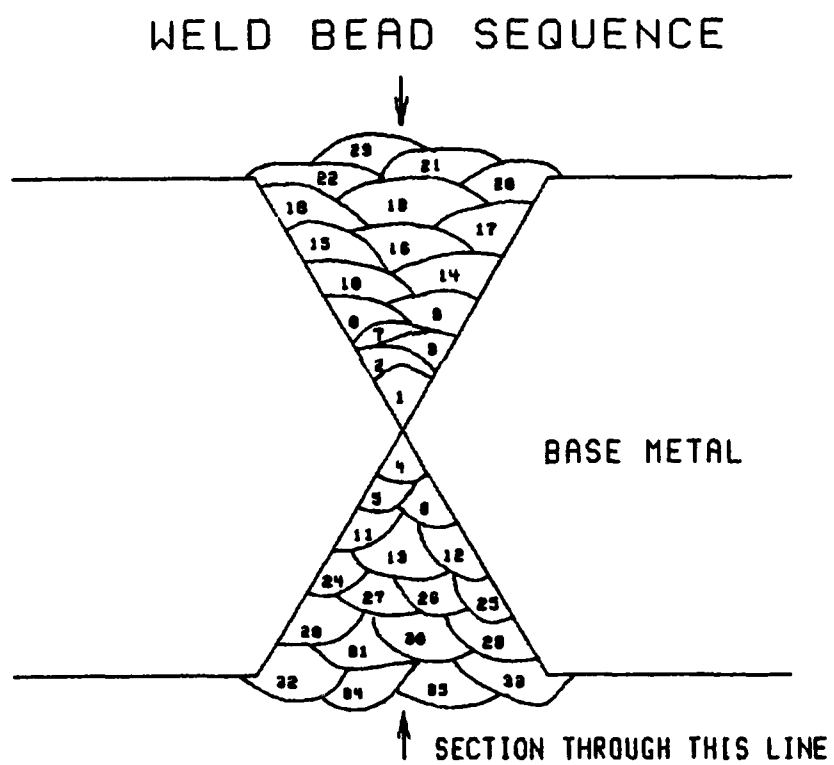
Figure 12
Schematic of multipass HSLA GMAW sample weldment.

42

.56"

SECTIONED AND POLISHED

SECTION "S"

SECTION "R"

2.0"

BASE METAL

FILLER METAL

FUSION BOUNDARY
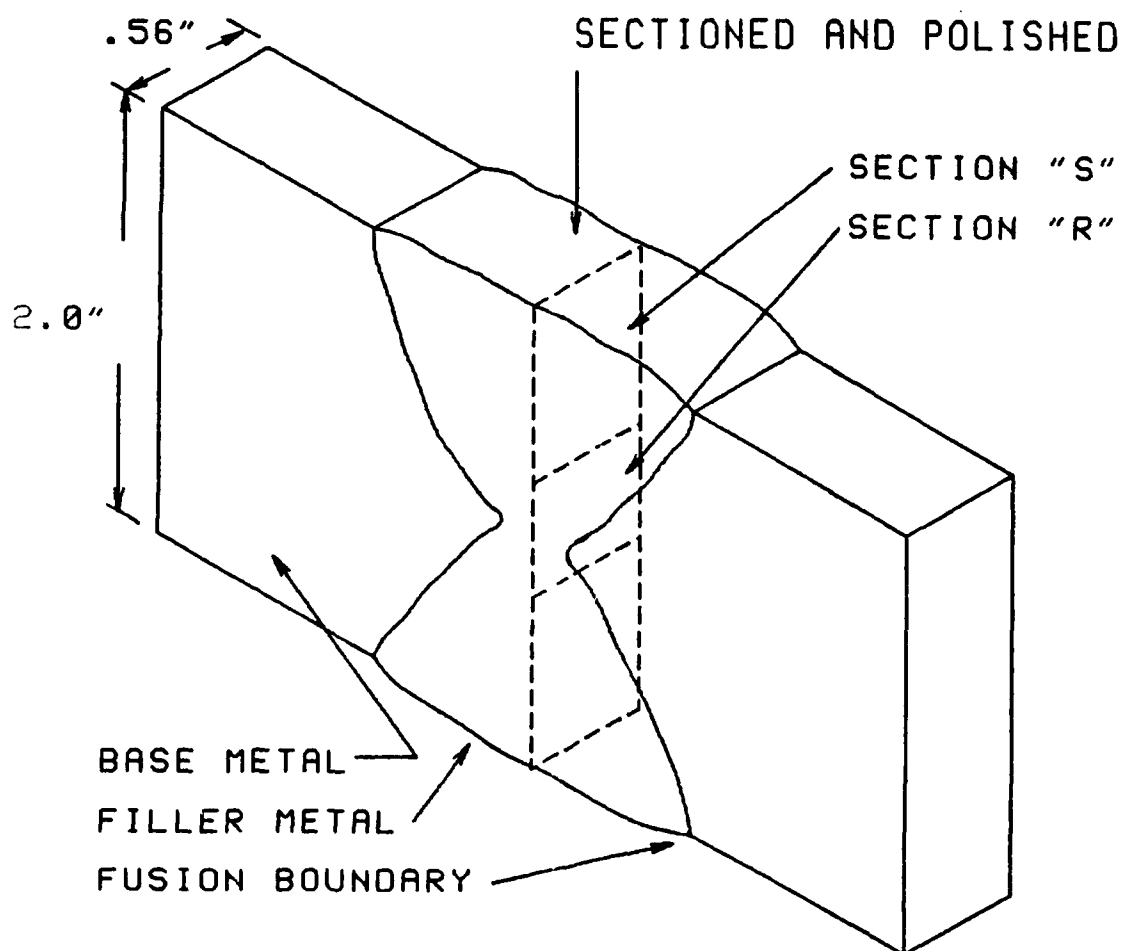
HSLA-100 GMAW WELD SAMPLE

Figure 13
Sectioning of HSLA sample weldment.

43

B. OPTICAL MICROSCOPY

The technique for obtaining micrographs of the weld regions "R" (vicinity of the root pass) and "S" (vicinity of the final pass) was identical to that described previously. One hundred fields were taken of each section.

Visual examination of the optical micrographs yielded some anticipated observations. The weld material of course underwent no mechanical processing after solidification. Thus the inclusions were uniformly circular in cross section (spherical).

The inclusions were of a roughly uniform small size and coloration. It was not possible to visually identify any distinctly different inclusion types such as oxides and sulphides from size, shape or coloration. The small size of inclusions (as compared to the ASTM 9260) material and especially the absence of large globular MnS inclusions was expected due to the agitation and high solidification rate present in the weld pool. The size of the inclusions present was in fact near the useful measurable limit of this technique. Comparison of the results of this analysis (See Table IV, Figs. 14-15) and the results from the ASTM 9260 samples demonstrates the apparent uniformity of inclusion size in the weld samples as compared to the wide distribution of sizes found in the fairly "dirty" spring steel. However, this presentation of the data may be somewhat misleading as inclusions smaller then approximately 0.5 microns are not all included.

The results tabulated are in fact somewhat suspect due to the uncertainty of the location of the lower tail of the distribution of inclusion sizes. The overall small size of the inclusions in the weld material resulted in the majority of inclusions identified being at, or near, the limit of resolution of this technique. Presumably a large number of inclusions much smaller than this went unnoticed. The literature reviewed in fact
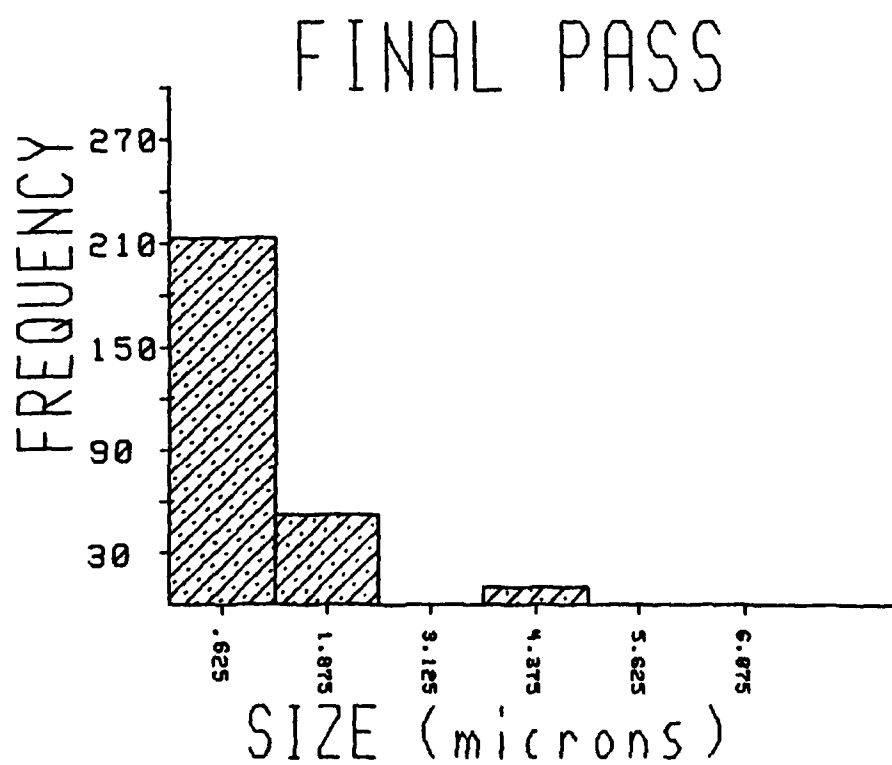
44

TABLE IV

ROOT PASS

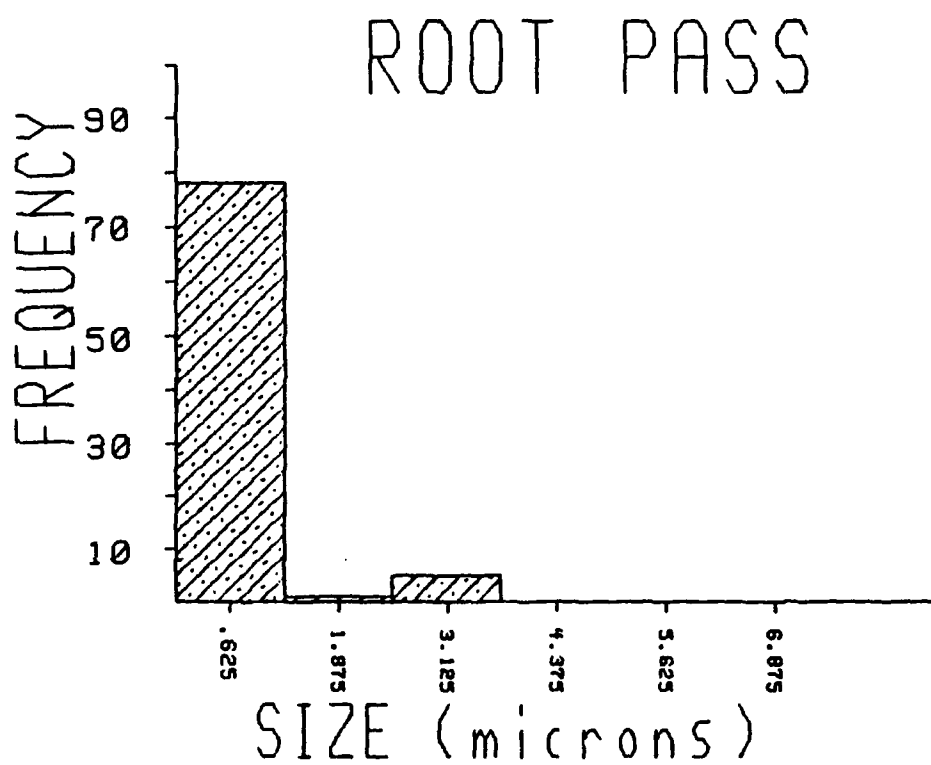|	
MEAN DIAMETER	.80±.05 microns
AREA FRACTION	.003%
MEAN SEPARATION	148 microns

FINAL PASS

MEAN DIAMETER	1.0±.1 microns
AREA FRACTION	.015%
MEAN SEPARATION	80 microns

Summary of results of optical microscopy of HSLA-100 weldment.

Figure 14
Distribution of inclusions in the final weld pass.

Figure 15
Distribution of inclusions in the root pass.

47

indicated the likelihood that the mean of the inclusion size distribution lies below this limit. The mean diameters calculated do indicate a somewhat qualitative trend towards larger size in the final weld pass.

C. EDX ANALYSIS

Energy dispersive X-ray analysis of inclusions in both the root pass and the final pass were carried out utilizing the technique described in Appendix C and analyzed as described in Appendix D.

Some general observations could be made from the observation of the samples in the SEM. Using the SE mode, it was apparent that a great number of inclusions of diameter less that 0.5 micron could indeed be found in both sections "R" and "S". These inclusions were of circular cross section. The higher magnifications available in the SEM revealed a definite substructure visible in many of the inclusions in the final pass which were often "marbled" in appearance (See Fig. 16).

The results of the EDX analysis are summarized in Tables V and VI. Note that the composition of the inclusion material was fairly uniform throughout each section. With the exception of inclusion "G" (the sole predominantly MnS inclusion identified in either section which, for this reason was dropped from the calculation of distribution of composition within section "R"), the composition of inclusions within section "R" is extremely consistent.

Comparison of the average inclusion composition indicates a statistically significant segregation of inclusion composition between the root and final pass. Inclusions within the root pass are predominantly (>98%) MnO, manganosite. In fact, manganosite occurs very rarely in steels in a pure form, but is found in combination with FeO.
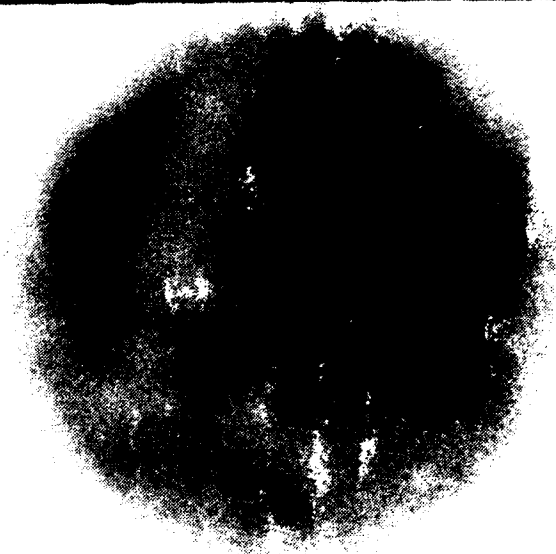
Figure 16
Inclusion "D" (Table VI) from the final weld pass.

49

TABLE V

INCLUSION	Si	S	Ti	Mn
A	--	0.4	--	82.2
B	0.1	--	0.1	91.3
C	4.1	--	--	70.0
D	3.2	--	1.1	79.4
E	--	0.3	--	78.1
F	--	--	--	96.0
G*	3.7	26.1	1.9	65.5
H	1.8	--	0.9	90.3
I	--	--	--	88.9
MEAN	1.2	--	0.3	84.7
σ	1.7	0.2	0.5	8.7
±(95%)	1.1	0.2	0.4	6.1

* (DROPPED, SEE TEXT)

Chemical composition of root pass inclusions.

50

TABLE VI

INCLUSION	Si	S	Ti	Mn
A	23.9	2.0	8.4	64.1
B	19.7	1.8	17.7	40.8
C	0.2	0.1	0.2	96.7
D	5.1	2.2	5.7	60.2
E	10.1	0.3	2.8	60.0
F	13.0	3.5	11.8	44.2
G	7.0	1.2	6.8	68.6
H	10.2	0.3	1.3	64.7
I	5.8	1.7	6.1	67.2
MEAN	10.6	1.5	6.8	62.9
σ	7.4	1.1	5.5	16.2
±(95%)	4.8	0.7	3.6	10.5

Chemical composition of final pass inclusions.

Unfortunately the small size of the inclusions and the consequent need to utilize the matrix stripping technique (See Appendix D) made it impractical to analyze the FeO content. We can safely assume that in a steel of this moderate (.75%-1.05%) Mn content, MnO is not present in pure form, but as a constituent of a MnO-rich, FeO-MnO phase.

Inclusions in the final pass exhibited a different composition. Ti and Si deoxidation products were found to be present in concentrations of 6.8 and 10.6 atomic percent, respectively. For the "average" inclusion, this would indicate a weight percent composition of 78.7% MnO, 11.5% SiO_2, and 9.8% TiO_2. While some (Metal)O-SiO_2-TiO_2 inclusions have been observed in steels, they are fairly uncommon. MnO-TiO_2 inclusions have been identified as well as MnO-SiO_2 phases. TiN inclusions are observed in steels, however these inclusions are normally of a polygonal geometry not observed in the inclusions in the weldment analyzed. The instrument used in this analysis was incapable of indicating the presence of nitrogen or oxygen (See Appendix B). The method of analysis used in this study made identification of FeO-TiO_2-SiO_2 combinations impractical. As mentioned prev isly, the inclusions observed in section "S" often exhibited a complex substructure or "marbled" appearance which in fact corresponded to a segregation of a Ti-rich phase within the inclusion body (See Figs. 16-17).

500 NM

Figure 17
X-ray map of Ti-rich region in inclusion in Fig. 16.

53

V. SUMMARY

A. CONCLUSIONS

1. Optical Microscopy

The results of the optical microscopy failed to yield significant quantitative information on the size distribution of nonmetallic inclusions between the root and final pass of this multipass weld. The mean inclusion diameter was almost certainly less than could be reliably measured with an optical microscope. While the calculated values for mean diameter of the inclusions in each region is somewhat suspect, it appears that the size of inclusions does decrease from the root pass to the final pass. This would appear to be consistent with the model of large inclusions composed of deoxidation products being concentrated in a hot zone near the surface of the weld where they are likely to be forced to the surface by agitation. Upon subsequent welding passes, these large inclusions would become essentially exogenous to the current weld and would exhibit greater flotation due to their larger size. Inclusions from previous passes would also serve as nucleation sites for coalescence of deoxidation products of subsequent welding passes.

2. EDX Analysis

The results of the EDX analysis tend to confirm this observation. Those inclusions which are near the surface of a weld pass when it solidifies may then act as nucleation sites for the creation of larger oxide inclusions upon remelting in each subsequent welding pass. The oxygen present in the shielding gas will continue to provide a source of dissolved oxygen in newly deposited weld metal. The formation

energy of TiO_2 and SiO_2 indicate that Ti and Si will react with the dissolved oxygen from this source. The small amounts of Ti and Si present in parent and filler metal would immediately react with dissolved oxygen (in preference to Mn which is a less powerful deoxidant). The work of Grong et al. (see p.16) indicates that the mean inclusion size in this high Mn:Si ratio steel should be very small. The relatively larger size of inclusions in the final pass is then explained by the subsequent remelting and coalescence of these oxides with other deoxidation products.

This growth process is further indicated by the observation of many complex inclusions near the surface, where fine Ti and Si deoxidation products have become agglomerated into a larger mass which exhibits a substructure of nonuniform composition.

SiO_2 and TiO_2 phases are certainly also present in the root pass as very fine inclusions smaller than 0.5 microns.

B. RECOMMENDATIONS

Nonmetallic inclusions play an important role in the strength and toughness of welds in HSLA steels. Active research on the effects of inclusions on welding of these products is ongoing at several institutions throughout the country. The current U.S. Navy program aimed at certification of a series of HSLA steels to replace the HY steels, and the development of suitable welding processes and consumables, encourages pursuit of further research in these areas.

The small size of the inclusions encountered in weld metals demands the use of extremely sensitive tools in their study. The analysis of the composition and identification of inclusion phases present is significant in the role they play in the nucleation of the final microstructure. Study of inclusions of 0.5 micron and less in

55

diameter, demands the use of the transmission electron microscope (TEM) and appropriate EDX analysis tools.

An integral part of this study was the development of a technique suitable for study of these small inclusions with the equipment available. This technique has been demonstrated. Further study involving the comparison of inclusions within SAW or SMAW welds of similar base material can be conducted with this technique and should prove valuable.

APPENDIX A

OPTICAL MICROSCOPY

The photomicroscope used in this study allows adjustment of light, aperture and shutter speed in order to take 35mm photographs with various films and lighting conditions. Details on the operation of the microscope are contained in the operator's manual. The settings for various magnification and viewing procedures will of course vary. Thus the settings, films and procedures discussed in this appendix are those used only in this study.

The samples were first observed to determine the magnification which would be used. The lowest magnification which gave adequate resolution was selected in order to attain maximum sharpness and depth of field. Using the ASTM 9260 samples as controls, the best magnification was determined to be X200. Note that the magnification in the optical path and photographic light path differ. Magnification is determined by the eyepieces, objective and "Optivar" lens setting. Charts are available in the operator's manual giving effective magnification for various settings for both the optical and photographic path.

The proper light and shutter speed settings can be approximated from the tables provided in the manual. Once the proper settings are determined a series of "test" shots are made while varying each parameter within the listed range and recording all settings. The best settings can then be selected from this sequence. In this study Kodak Pan X ASA 125 black and white film was used. The following settings were used on all photographs.

- SHUTTER SETTING - "5"

57

- APERTURE - "B"

- LIGHT METER - "V"-"VI"

The sample should be oriented in the micrometer holder such that the desired number of fields can be photographed in "strips" by systematic adjustment of the micrometer. Suppose 100 fields are to be taken of a rectangular sample. The fields can be selected by starting at one corner of an imaginary box, advancing fields using one axis of the micrometer for 25 fields, traversing with the orthogonal axis of the micrometer and advancing in the opposite direction. Four passes in this manner will complete 100 fields (See Fig. 10).

APPENDIX B

SCANNING ELECTRON MICROSCOPE

The SEM was used primarily to investigate the composition of inclusions through the EDX equipment and software. However, the SEM itself allows several modes of observation which were used in this study. Each mode takes advantage of a different form of interaction between the electron beam and the sample. These modes are described briefly below.

The secondary electron (SE) mode was used for nearly all general observation and location of inclusions. Bombardment of the sample by the focussed electron beam results in inelastic collisions with the atoms of the sample material. Low energy secondary electrons are then expelled with an energy much less than that of the incident beam. The electron beam is scanned over the surface of the specimen and the emitted secondary electrons are collected and processed as a signal in order to generate an image of the scanned surface on a CRT screen. The emission of secondary electrons is heavily influenced by the physical geometry of the incident surface. The image generated is thus useful for studying the details of surface contour.

The backscattered electron (BSE) mode is very useful for obtaining contrast on objects consisting of different materials even with little or no surface contour difference. Backscattered electrons are generated by elastic, or nearly elastic, collisions of incident beam electrons with sample nuclei. The intensity of such high energy electrons emitted form the sample is thus highly dependent on the atomic number of the atoms present in the target area. The backscattered electrons are collected by a separate detector and processed as a signal to be displayed on the CRT. The backscattered electron mode is

59

very useful for observing areas of different atomic number on the surface of a sample such as inclusions on the surface of a polished specimen or phases within such inclusions.

The SEM can also be used in the energy dispersive X-ray (EDX) analysis mode. High energy electrons of the incident beam may impart sufficient energy in collisions with target atoms to remove an innermost K-shell electron. Electrons from within the atom will then lose energy to fill this vacancy, emitting X-rays. The energy of the X-rays emitted in this process (known as "K-capture") is unique for different elements and can be used to identify the presence of these elements. The X-rays are collected by a detector and the resulting signal can be analyzed with appropriate software in order to identify the elements present. There are two significant restrictions to EDX analysis. The source of the X-rays in the analysis is actually an area somewhat larger than the diameter of the incident electron beam and actually extends below the surface features observed. The system used in this study was restricted to analysis of elements of atomic number greater than 11 (sodium, Na) due to absorption of the characteristic X-rays from lighter elements by the detector window. Thus oxygen, nitrogen, carbon and boron go undetected.

APPENDIX C

ENERGY DISPERSIVE X-RAY ANALYSIS

Energy dispersive X-ray spectra were collected and manipulated with the KEVEX Analyst. Inclusions were analyzed qualitatively and quantitatively with this equipment. Important limitations of this analysis include the fact that the resolution of the instrument (a function of the excited X-ray producing volume in the sample) may in some cases actually be larger than the inclusions being observed. The instrument is not capable of indicating the presence of oxygen, nitrogen and other light elements (see discussion in Chapter III). Also , the X-ray signals produced do not necessarily correspond to that portion of the sample observed on the CRT. With these limitations in mind, quite useful information can be gained through a combination of the EDX data with thermodynamic considerations. The reduction of EDX data utilizing free energy of formation and phase equilibria is considered in Appendix D.

The procedure utilized for collecting EDX spectra is outlined below, followed by a brief discussion of useful options for manipulation of the data with the available software. Detailed operating instructions are available in the instruction manual. A short list of useful commands is included at the end of this appendix.

Prior to analysis of the sample, the system must be calibrated with a standard. The software contains an autocalibration routine which allows the equipment to be calibrated via a copper/aluminum reference.

With the system calibrated, the sample can be viewed (SE mode) in order to locate inclusions. Once the first inclusion is located some adjustments can be made in order to facilitate data acquisition. The vertical axis should be adjusted in order to attain a

uniform working distance of approximately 30 mm. This done, the detector can be activated and the spot adjusted to achieve an X-ray detector reading of approximately 1500 counts per second. Once this has been accomplished, only minor adjustments should be necessary in order to maintain these operating values. These values were found to give the most reliable results with the ASTM 9260 samples.

Once an inclusion has been located, the adjustments made and a spectrum collected, this spectrum data can then be saved to a memory tape. It is recommended that spectra be collected on the desired number of inclusions in each sample and saved for later analysis. This ensures consistency of the operating performance of the equipment and the sample surface quality, as well as saving time.

The KEVEX software allows a number of useful operations to be performed on the stored spectra. Some are required for useful interpretation of the data, others may used to process or refine data which might otherwise be ambiguous.

In some cases it may be useful to remove the matrix material peaks from a spectrum. This is done by saving a spectrum of the local matrix material and another of the inclusion. The two spectra can then be linearly scaled and summed, thus effectively "stripping" the matrix from the combined matrix/inclusion spectrum (See Fig.C.1).

In order to obtain a useful analysis of an X-ray spectrum, the continuum background of X-ray radiation must be removed. The software contains a routine which removes this background.

Peaks for some elements may overlap. The software also contains a deconvolution stripping routine which allows separation of peaks approximated as Gaussian curves.
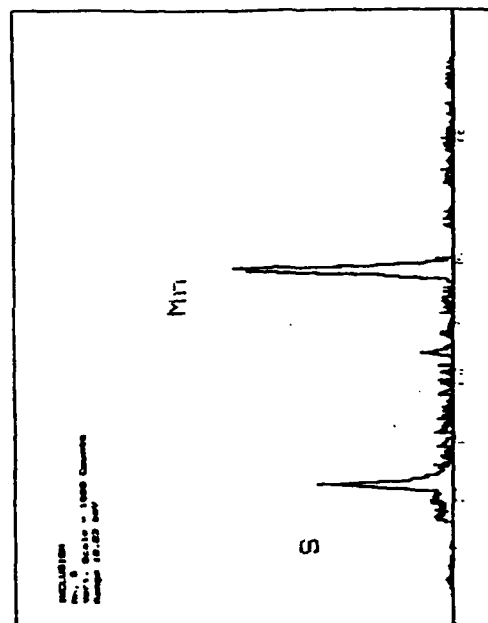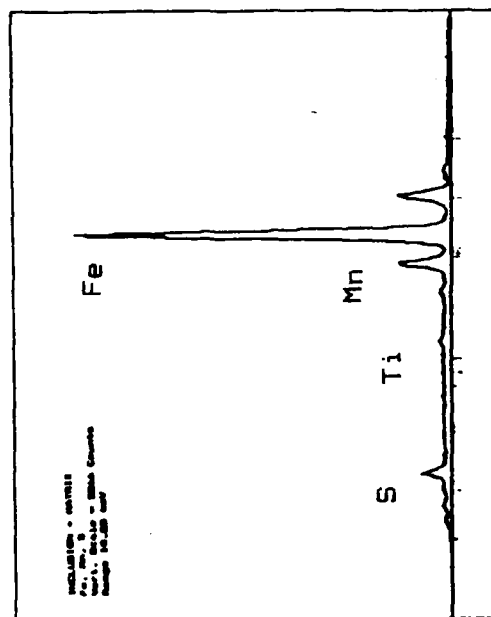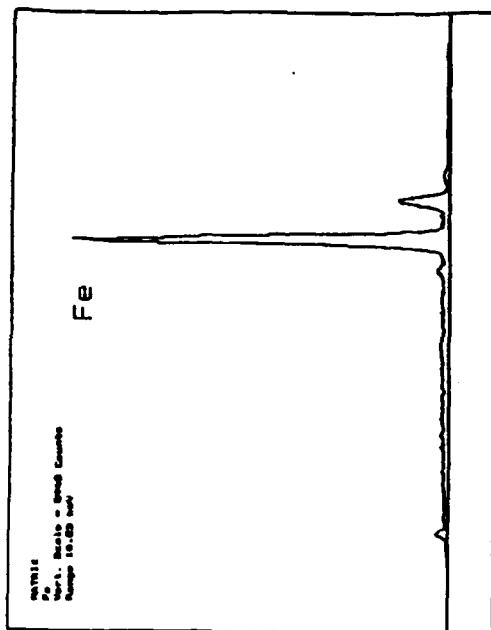
Figure C.1
Reduction of inclusion EDX spectra (see text for details).

63

Finally, the software also contains automatic routines for applying corrections for the effects of 1) atomic number and its effect of energy dissipation 2) absorption of X-rays generated within the excitation volume and 3) fluorescence or emission of X-rays by one atom as a result of the absorption of a higher energy X-ray emitted by another. Taken together these corrections are known as ZAF corrections.

The following list contains some of the more useful KEVEX commands and macro-commands used to perform some of the operations described in this appendix.

- <ACQUIRE> - gathers spectrum data from the detector in the SEM chamber.

- <CLEAR> - clears old data from the screen.

- <MLK> - automatically identifies peaks in a collected spectrum.

- sa/sp - saves a spectrum to memory.

- pro/ecs - removes escape peaks from a spectrum.

- bac/sub/auto - removes background from entire spectrum.

- bac/sub/nor - removes background from a selected region of the spectrum.

- id/li - sets list of elements to perform quantitative analysis on.

- ru/ex,pbaq - reduces background, removes escape peaks, performs analysis on selected elements, prints results.

- ru/ex,noprint - same as above except doesn't print results.

- decon/gauss - deconvolution subroutine, peaks approximated as Gaussian curves.

- re/sp,<name> - ENTER
  re/sp/over - ENTER
  pro/add - by entering the spectrum of the matrix material and the spectrum of the desired inclusion, this series of commands removes the peaks due to the matrix from the inclusion spectrum.

APPENDIX D

ANALYSIS OF DATA

A. DEVELOPMENT OF PROCEDURE

The purpose of this appendix is to present a general step by step procedure for the analysis of optical and EDX data such as that produced in this study. The procedure was developed with data collected from the ASTM 9260 test pieces. The size, distribution and compositions of inclusions in this high silicon spring steel (See Table D.1) are both predictable and well documented so samples of this material were actually used as a "standard" in order to calibrate the procedure.

B. ANALYSIS OF OPTICAL DATA

The sample was sectioned and prepared as described elsewhere. One hundred total micrographs were obtained. The photographs were divided into four groups (A,B,C,D) of 25 photographs each. Each group was shot in a separate area of the sample with Groups A and B shot perpendicular to the rolling axis and C and D shot parallel to the rolling axis. In the case of the ASTM 9260 test pieces, this treatment served to differentiate data sets based on orientation. It was anticipated that the differentiation for the weld series would be based on location within the fusion zone, each group comprising a series of photographs taken at various distances from the fusion boundary.

The first step in analyzing the photographs was to determine the final scale of the printed photographs. The developed film was shot at X200 magnification. Easily

TABLE D.1

ELEMENT	%
CARBON	.56-.64
MANGANESE	.75-1.00
PHOSPHORUS	<.035
SILICON	1.80-2.20
SULPHUR	<.04

Chemical composition of ASTM 9260 steel.

discernible features were then selected on the final photographs and the film and used to produce a scaling ratio. The printed photographs were four times the scale of the film, resulting in an overall magnification of X800.

The photographs were sorted in order to determine the size bins as described earlier. This cursory examination also made it clear that it would be necessary to divide the inclusions into two groups; large heavily deformed sulphides, and other smaller less deformed inclusions presumed to be oxides of some sort. The sulphides were easily identified in the micrographs from their gray coloration and elongation along the rolling axis. The unscaled image size of the smaller inclusions ranged from less than 2.0 mm to about 10.0 mm, sulfides ranged from about 4.0 mm to about 30.0 mm. These size ranges were divided into eight equal "bins" and all photographs were examined and measurements were taken.

Simultaneously a number of other pieces of data were gathered. First the aspect ratio (long axis:short axis) of the deformable MnS inclusions was determined. Second, the number of MnS inclusions apparently nucleated by other inclusions was tallied. The raw numbers of inclusions in each size bin (converted to actual size) is included along with the mean aspect ratio of the MnS inclusions in Tables D.2-D.3. The inclusion size distribution is often plotted in the form of a histogram (See Figures D.1-D.3). Note that the oxide inclusions are all grouped together on one graph due to their similar size and essentially spherical symmetry. The MnS inclusions are plotted on two separate graphs reflecting the two different orientations which result in considerable difference in sizes and aspect ratios. The mean and standard error of the discrete data groups are also calculated (See Table D.4). The area fraction for Groups A and B is calculated by using
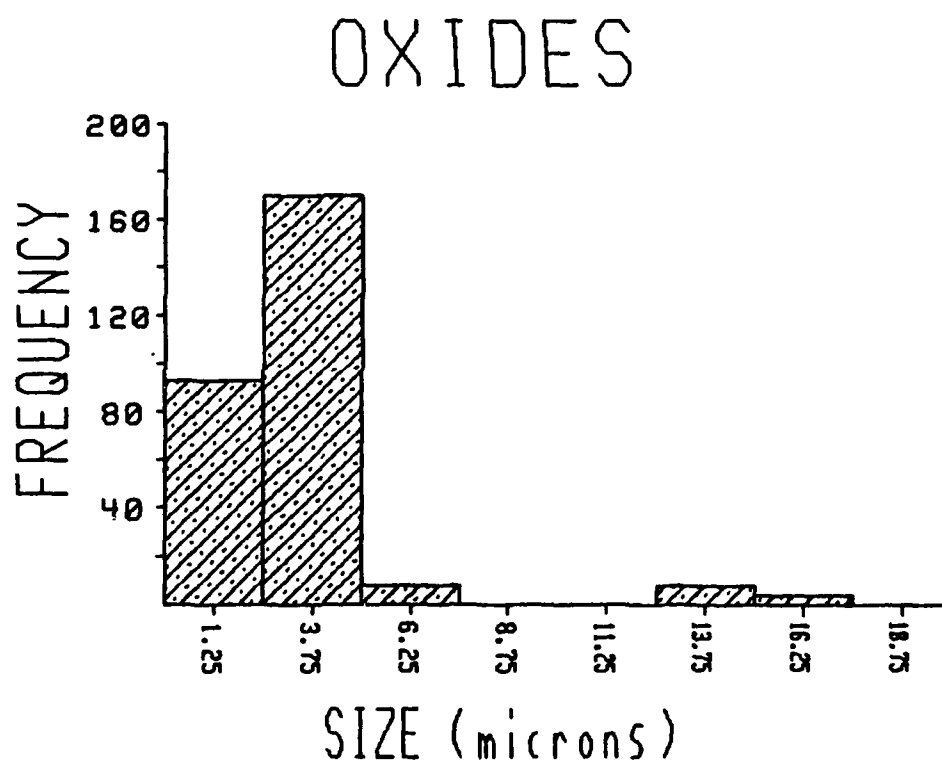
TABLE D.2

SIZE (microns)	GROUP			
	A	B	C	D
0-2.5	11	30	12	32
2.5-5.0	53	54	21	42
5.0-7.5	1	1	0	5
7.5-10.0	0	0	0	0
10.0-12.5	0	0	0	0
12.5-15.0	0	0	0	2
15.0-17.5	0	0	0	1
17.5-20.0	0	0	0	0

Oxide inclusions in ASTM 9260 sample.

TABLE D.3

SIZE (microns)	GROUP			
	A	B	C	D
0.0-5.0	15	9	3	0
5.0-10.0	7	5	5	2
10.0-15.0	3	4	1	3
15.0-20.0	4	0	0	5
20.0-25.0	0	0	0	1
25.0-30.0	0	0	2	4
30.0-35.0	0	0	0	0
35.0-40.0	0	0	7	0
MEAN ASPECT RATIO	1.5	1.7	0.9	10.4
NUCLEATED ON OXIDES	6	13	11	11

Sulphide inclusions in ASTM 9260 sample.

69

Figure D.1
Distribution of oxide inclusion size in ASTM 9260 steel sample.
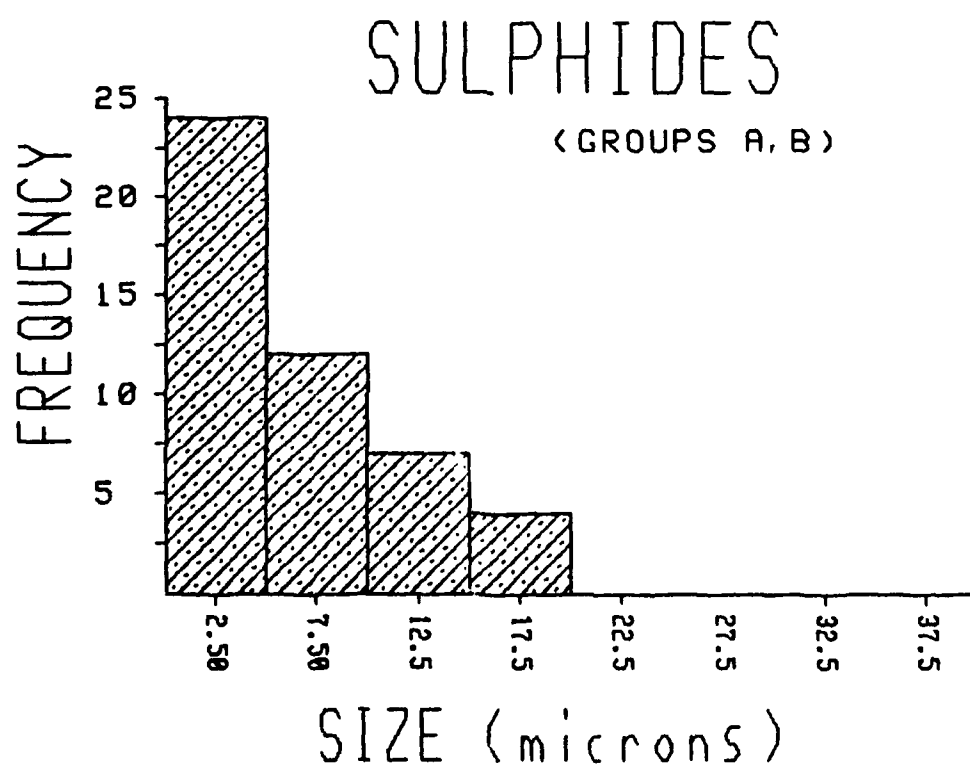
Figure D.2
Distribution of sulphide inclusion size in ASTM 9260 steel.
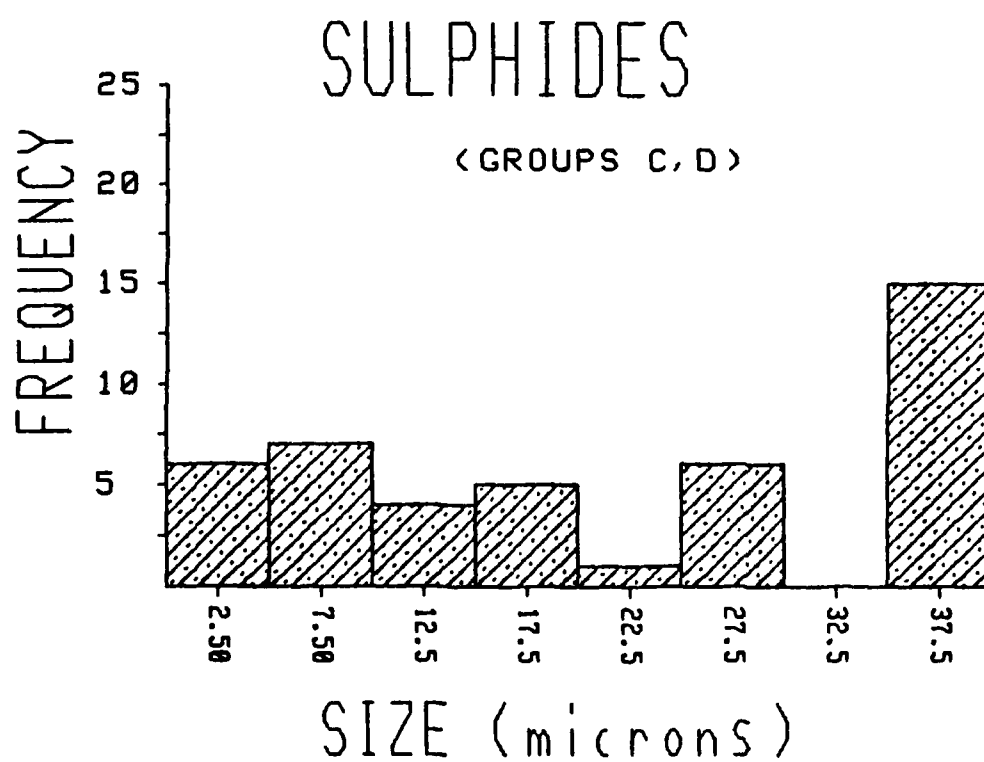
Figure D.3
Distribution of sulphide inclusion size in ASTM 9260 steel.

72

TABLE D.4

OXIDES

MEAN DIAMETER	$3.1 \pm .4 \times 10^{-6}$ M.
AREA FRACTION	.12%

SULPHIDES [*]

MEAN DIAMETER	$7 \pm 1 \times 10^{-6}$ M.
AREA FRACTION	.22%

MEAN SEPARATION 85×10^{-6} M.

(OXIDES)

---

[*] GROUPS A AND B ONLY

Summary of inclusion size data for ASTM 9260 sample.

73

the mean inclusion diameter (and assuming that all inclusions are circular in cross section), total number of inclusions in those groups and the total area photographed. Again the highly deformed nature of the MnS inclusions parallel to the rolling axis resulted in Groups C and D being dropped from this calculation. Finally, the average distance between inclusions was calculated for the Group A and B data. In this case the assumptions were the same as those used for the area fraction calculation with the additional assumption that the inclusions were distributed uniformly throughout sample fields.

C.   ANALYSIS OF EDX DATA

The EDX data was interpreted in the following manner. Spectra were collected on representative inclusions of both types near the mean size determined for each. Analysis of the sulfides was of course fairly straightforward. The EDX analysis indicated a ratio of 50 atomic percent Mn and 50 atomic percent S for these inclusions. This would be expected as Mn and S combine stoichiometrically to form MnS. Examples of EDX analyses for simple MnS type inclusions are included in Table D.5. The analyses indicate a Mn content within two atomic percent of the S content in all cases. In most of the cases the indicated Mn content is slightly greater than the S content in the inclusion.

The smaller inclusions in all cases contained a preponderance of Si and some other metallic element combining to form metallic silicates of varying composition (See Table D.6). In some cases the compositions could be inferred from the phase diagram of the combination present (eg, $MgO-SiO_2$). In none of the inclusions examined were Si and Al both present as oxides in the same inclusion. This result is expected in an Al

74

TABLE D.5

INCLUSION	Mn	S	Mn:S
A	48.33	50.47	.97
B	33.84	35.73	.95
C	41.20	42.44	.97
D	30.05	31.83	.94

Chemical composition of sulphide inclusions in ASTM 9260 sample.

TABLE D.6

INCLUSION	Al	Mg	Mn	Si	S	Ca	Fe
A	—	33.41	—	62.01	--	--	4.58
B	57,00	—	21.30	—	19.04	2.57	--
C	41.15	11.41	19.07	—	22.72	5.65	--
D	53.14	—	19.10	—	16.54	2.16	9.86
E	39.05	7.93	18.12	—	29.95	5.13	8.81
F	—	36.70	—	60.60	—	--	2.70

Chemical composition of oxide inclusions in ASTM 9260 sample.

containing steel due to the formation energy of the Al deoxidation product. It is equally unlikely to find MnO and Al_2O_3. All Al_2O_3 inclusions identified appeared to have served as nucleation sites for MnS inclusions.

1. Example 1

Inclusion "A" in Table D.6 has the following atomic percent composition: Mg (33.41%), Si (62.01%), and Fe (from the matrix which was not removed in this case, 11.36%). From the known stoichiometries of MgO and SiO_2, the weight percent of each compound in the inclusion can be calculated. The result is 26.6% MgO by weight. This figure is used to enter the $MgO-SiO_2$ phase diagram which indicates a composition of $SiO_2+MgSiO_3$. Note the relatively low melting point of this silicate.

Many of the MnS inclusions were apparently nucleated around other higher melting point inclusions. The smaller crystalline inclusions identified within the MnS appear to be Al_2O_3 in most cases. Silicate inclusions were not identified in any case as nucleation sources for MnS. These inclusions were normally complex inclusions of Al and either Mn, Mg, or Ca. (See Table D.6). The phases present in such complex inclusions can be inferred from free energy and phase diagrams as follows (useful free energy and phase diagrams are included in Appendix E).

2. Example 2

Inclusion "B" in Table D.6 has the following atomic percent composition: Al (57.0%), S (19.04%), Ca (2.57%), Mn (21.39%). Looking at the free energy diagram for oxides, Ca, and Al oxides have a much greater (more negative) free energy of formation than Mn. Checking the free energy of formation of sulfides, it appears that Ca would react with any excess S not combined with Mn. However, the Mn:S ratio is very nearly 1:1 indicating that the Mn and S are probably all contained in MnS. Additionally, the

physical appearance of the sulfide inclusions suggests that CaS is not present. Effective shape control through Ca additions results in harder non-deformable sulfide inclusions which tend to retain a spherical shape during processing. This effect is not evident in this steel. It appears that the Al and Ca are both present as oxides. The mole ratios of Al and Ca can easily be calculated and, knowing the stoichiometries of CaO and Al_2O_3, the weight percent of the oxides can be calculated. Reference to the equilibrium phase diagram for $CaO-Al_2O_3$ indicates that the phase present should be C_3A_5 ($3CaO-5Al_2O_3$) and excess Al_2O_3.

3. Example 3

Inclusion "C" in Table D.6 has the following atomic percent composition: Mg (11.41%), Al (41.15%), S (22.72%), Ca (5.65%), and Mn (19.07%). The same observations as for inclusion "B" indicate that the Mn and S all occur as MnS and the Ca is present as an oxide. In this case Mg, Al and Ca all occur as oxides making it necessary to use the ternary phase diagram $MgO-Al_2O_3-CaO$. The weight percent of each of the component oxides is: $MgO-16.0\%$, $Al_2O_3-73.0\%$, and $CaO-11.0\%$. The phase diagram indicates that the material is very near the CA_6 with some spinel $MgO-Al_2O_3$ present.

APPENDIX E

EQUILIBRIUM PHASE DIAGRAMS

This appendix contains several useful equilibrium phase diagrams and free energy diagrams used in this study. Other equilibrium phase diagrams for systems commonly encountered in steelmaking can be found in Phase Equilibria Among Oxides In Steelmaking (Muan and Osborn, 1965) from which these were extracted.
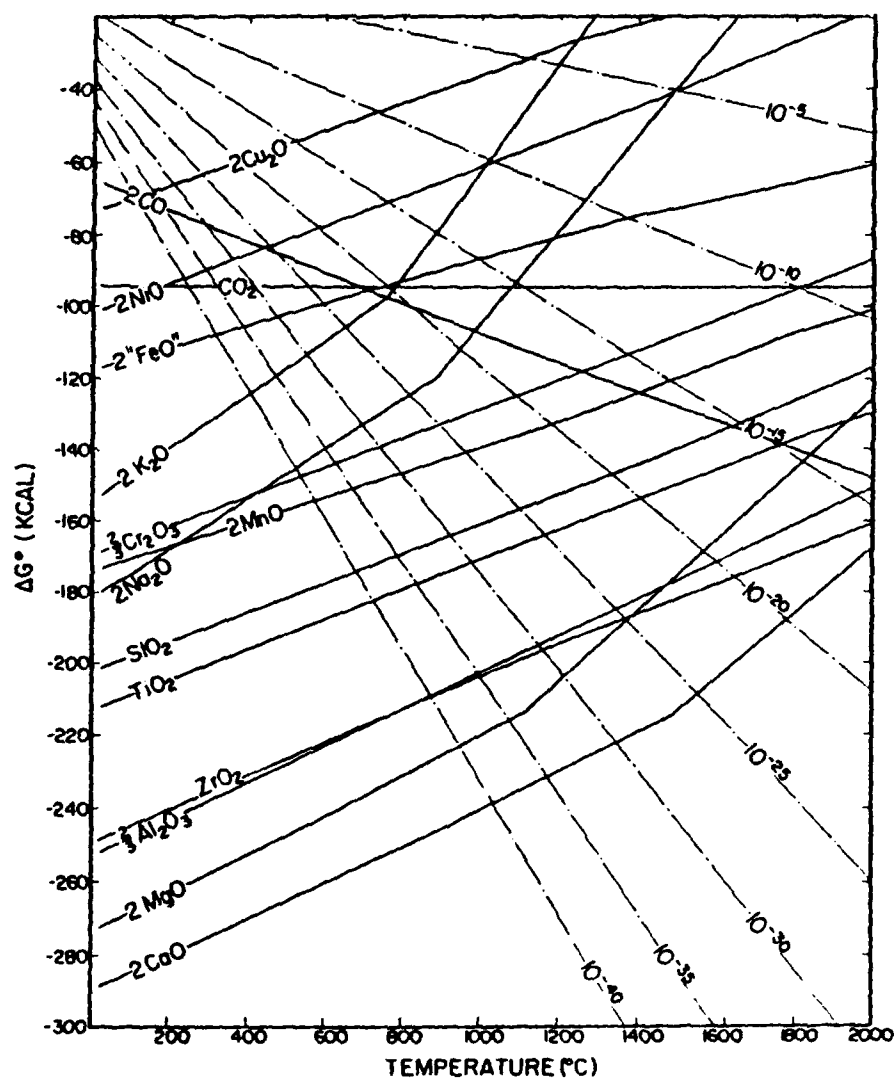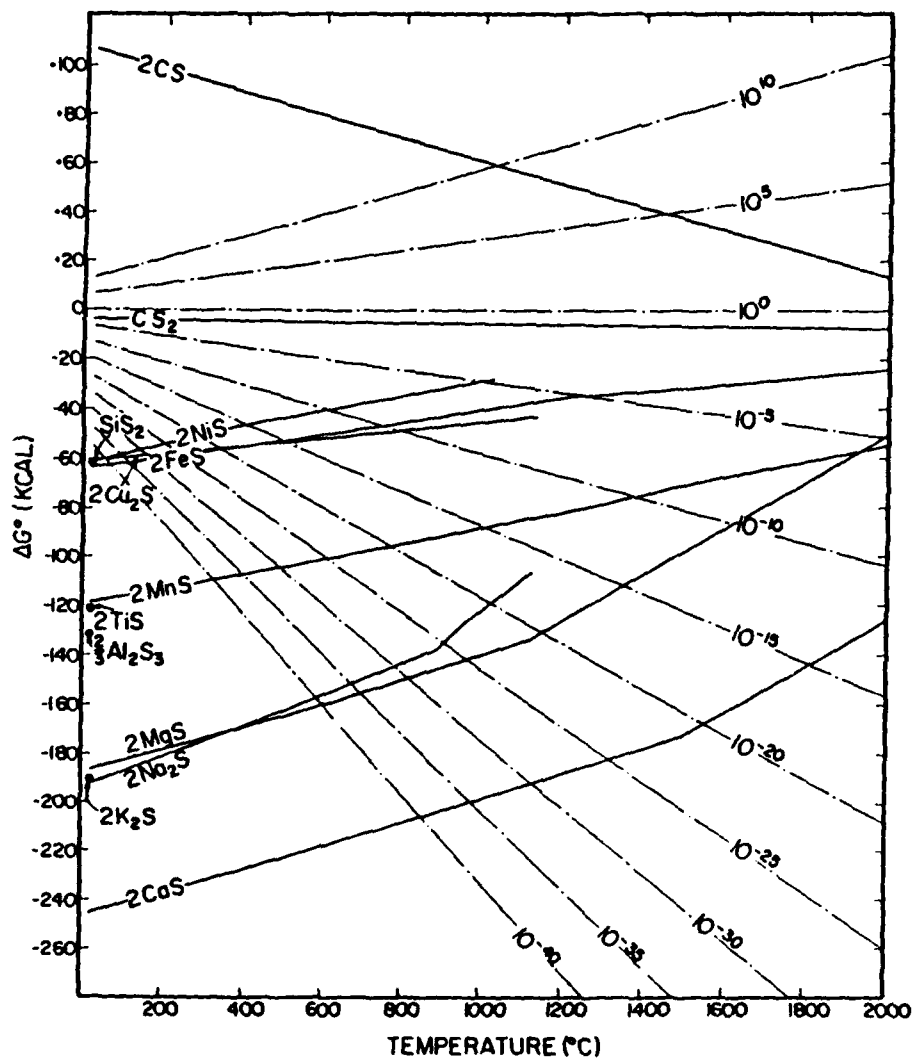
Figure E.1
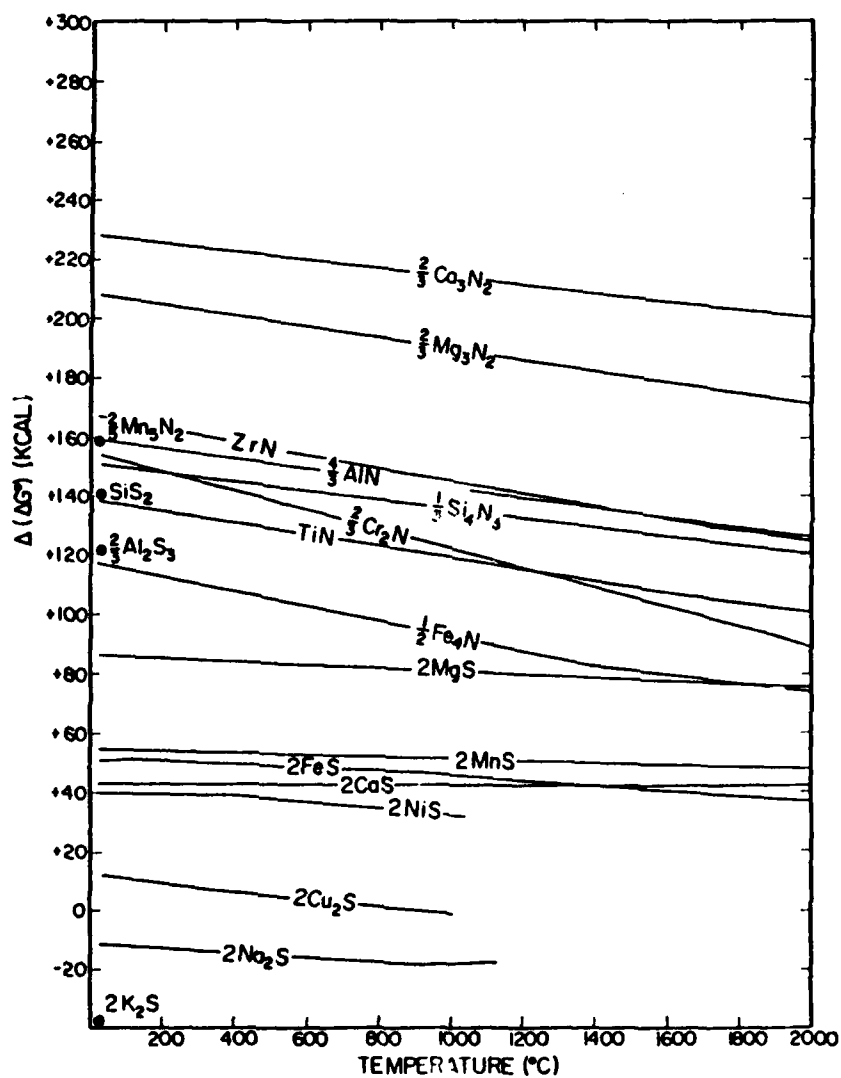Free energy of formation of oxides (Muan and Osborn, 1965, p.4).
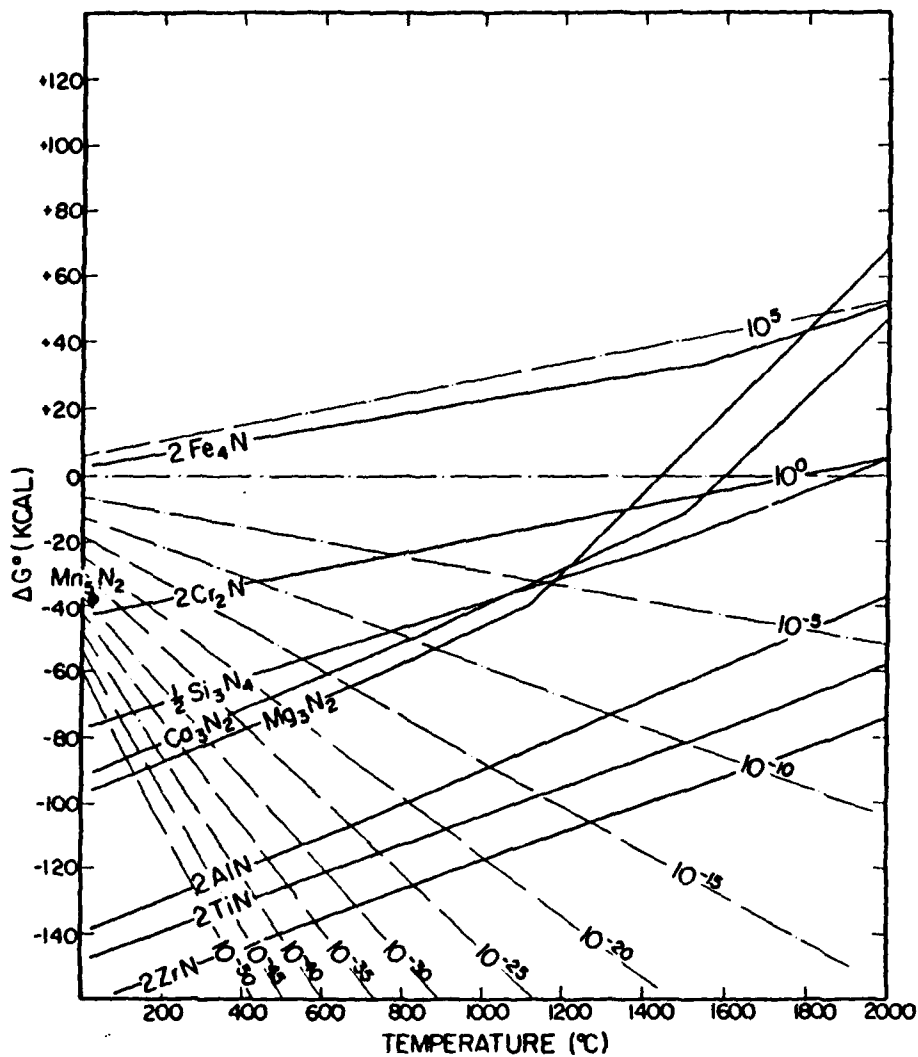
Figure E.2
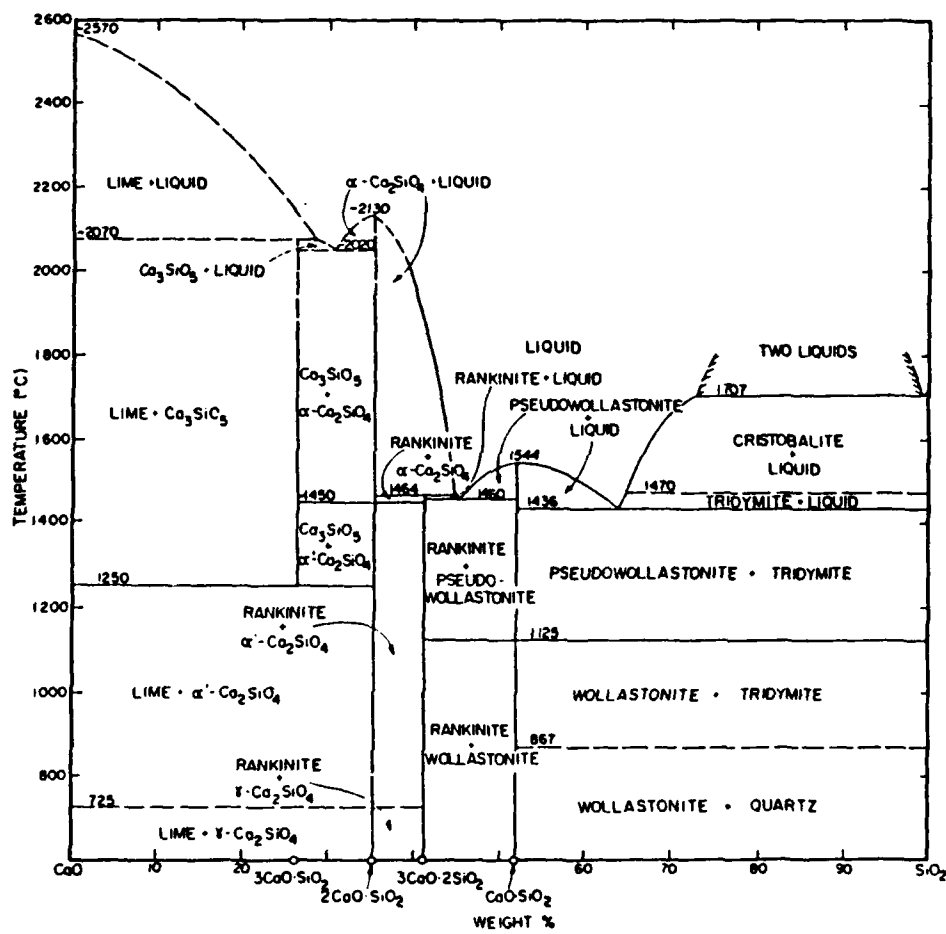Free energy of formation of nitrides (Muan and Osborn, 1965, p.9).

81

Figure E.3
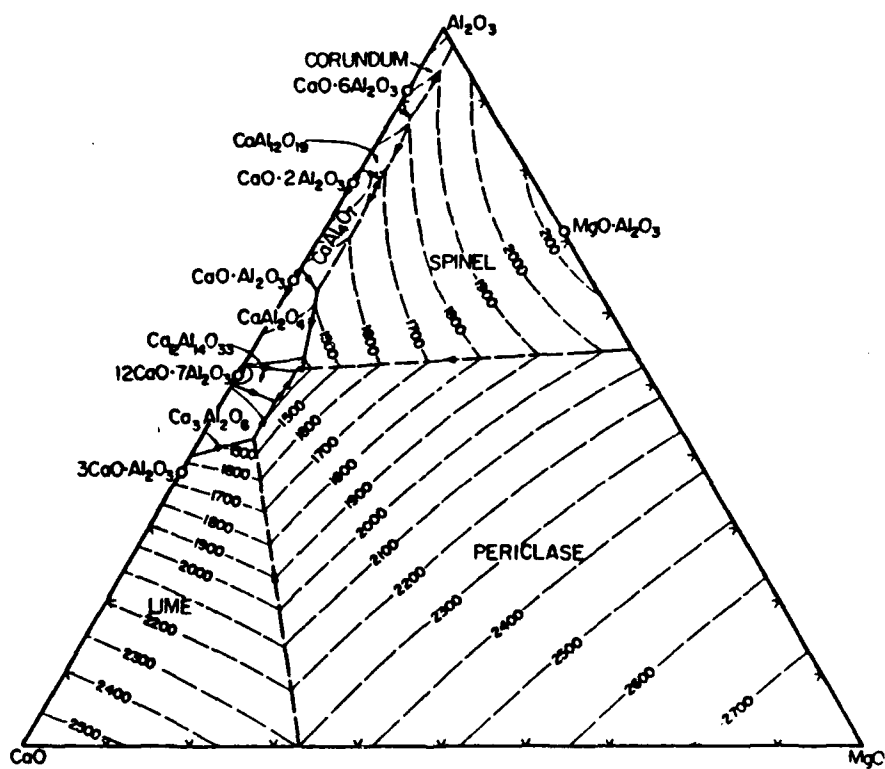Free energy of formation of sulphides (Muan and Osborn, 1965, p.8).

82

Figure E.4
Comparison of free energies of formation (Muan and Osborn, *1965, p.11*).
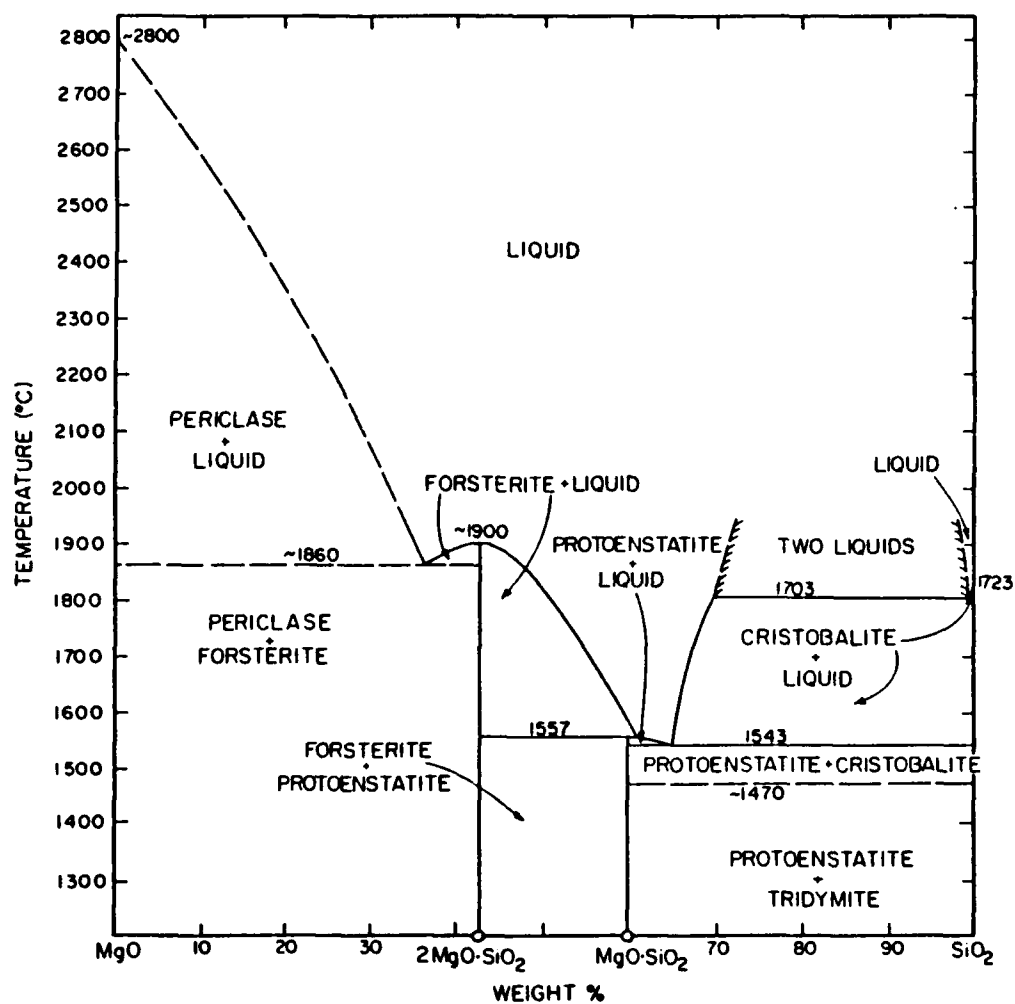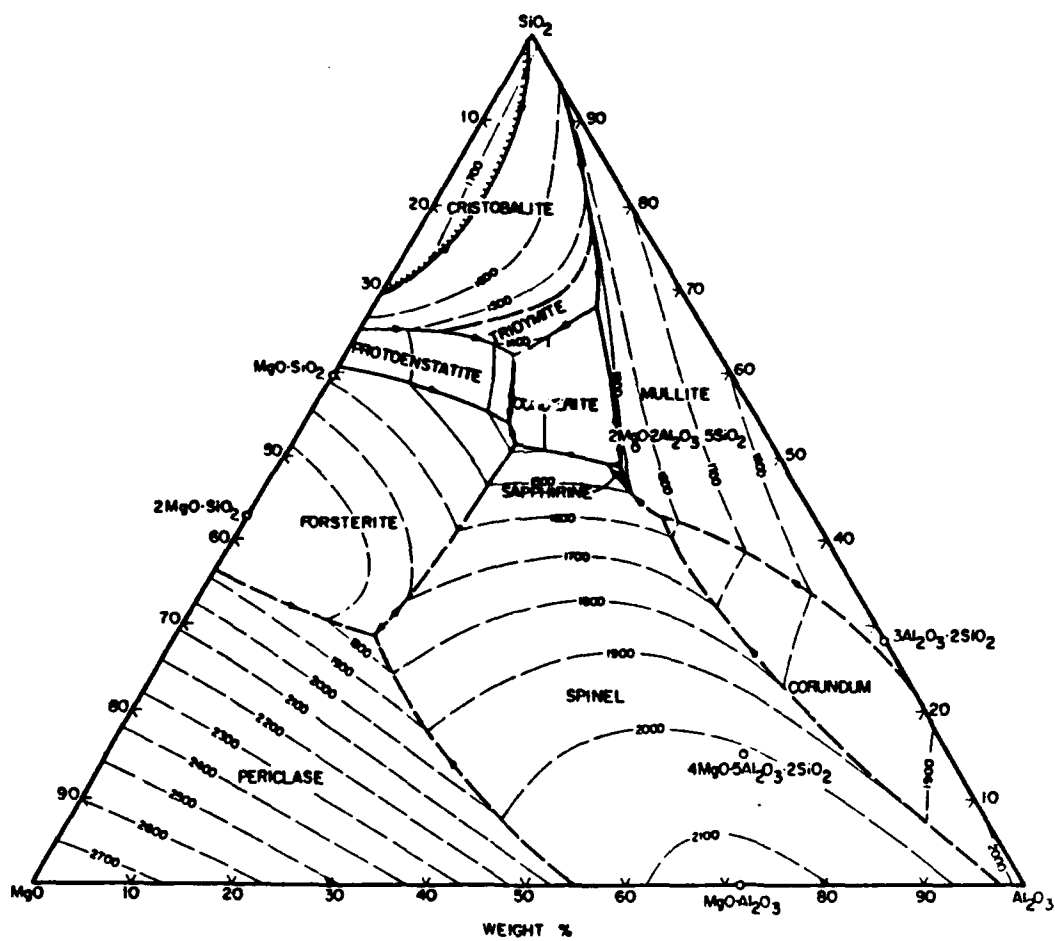
Figure E.5
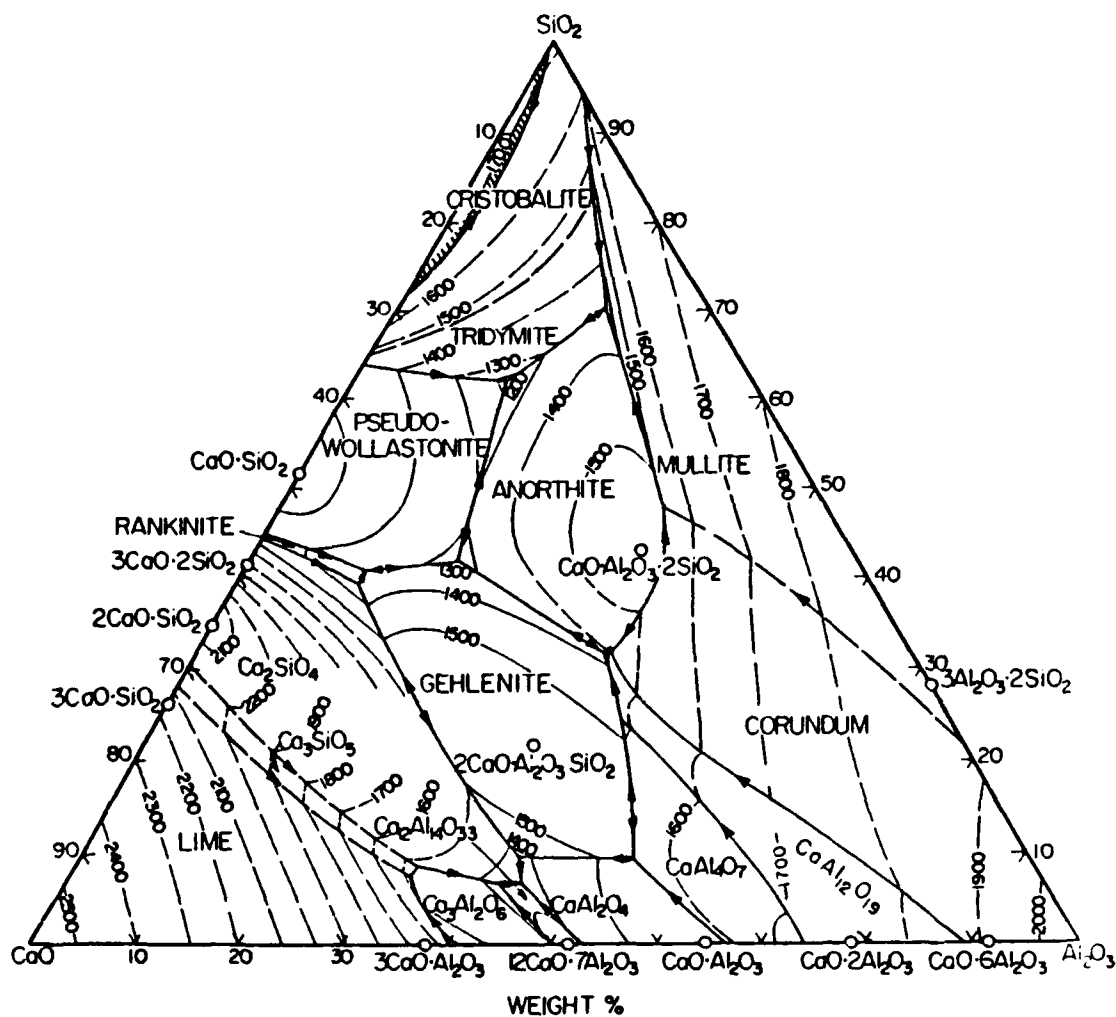Phase diagram MgO-SiO$_2$ system (Muan and Osborn, 1965, p.39).

84

Figure E.6
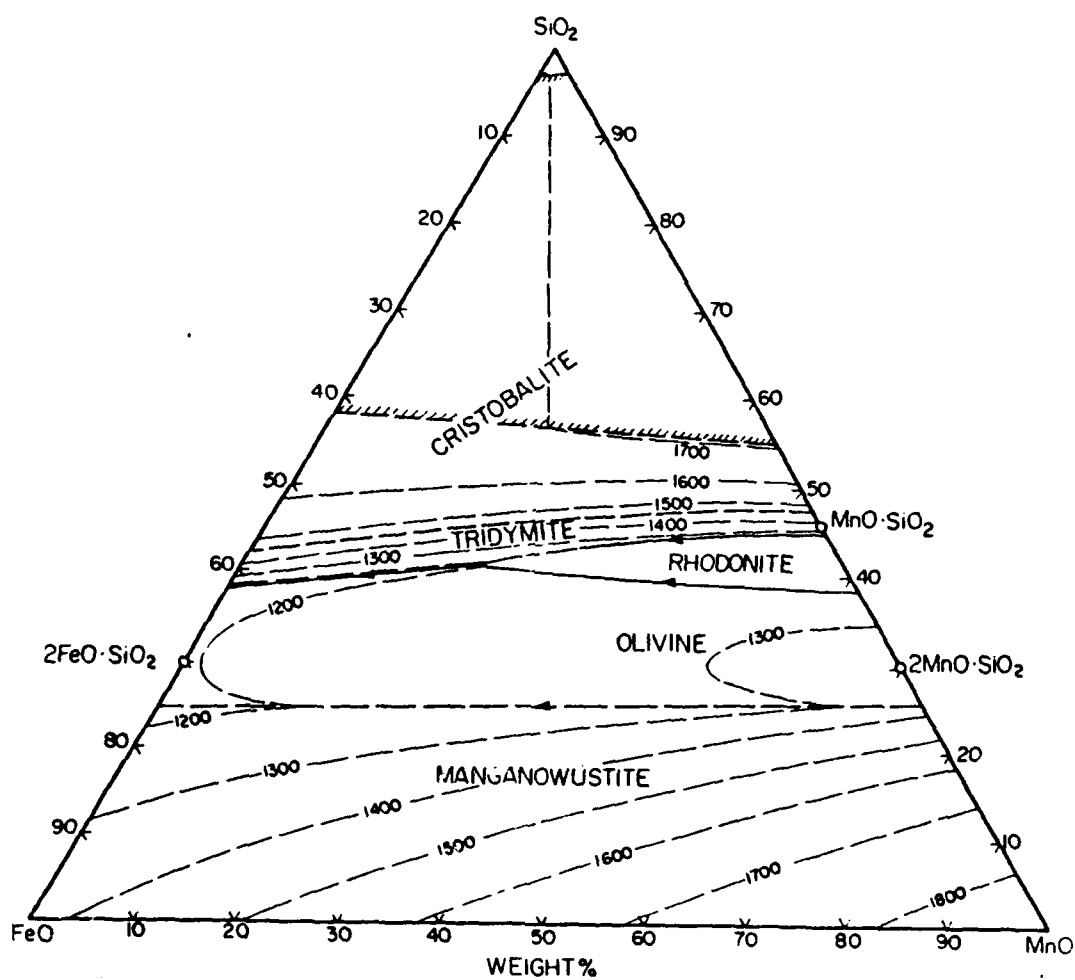Phase diagram CaO-SiO$_2$ system (Muan and Osborn, 1965, p.35).

85

Figure E.7
Phase diagram CaO-MgO-Al$_2$O$_3$ system (Muan and Osborn, 1965, p.92).

86

Figure E.8
Phase diagram MgO-Al₂O₃-SiO₂ system (Muan and Osborn, 1965, p.96).

Figure E.9
Phase diagram CaO-Al₂O₃-SiO₂ system (Muan and Osborn, 1965, p.93).

88

Figure E.10
Phase diagram FeO-MnO-SiO$_2$ system (Muan and Osborn, 1965, p.121).
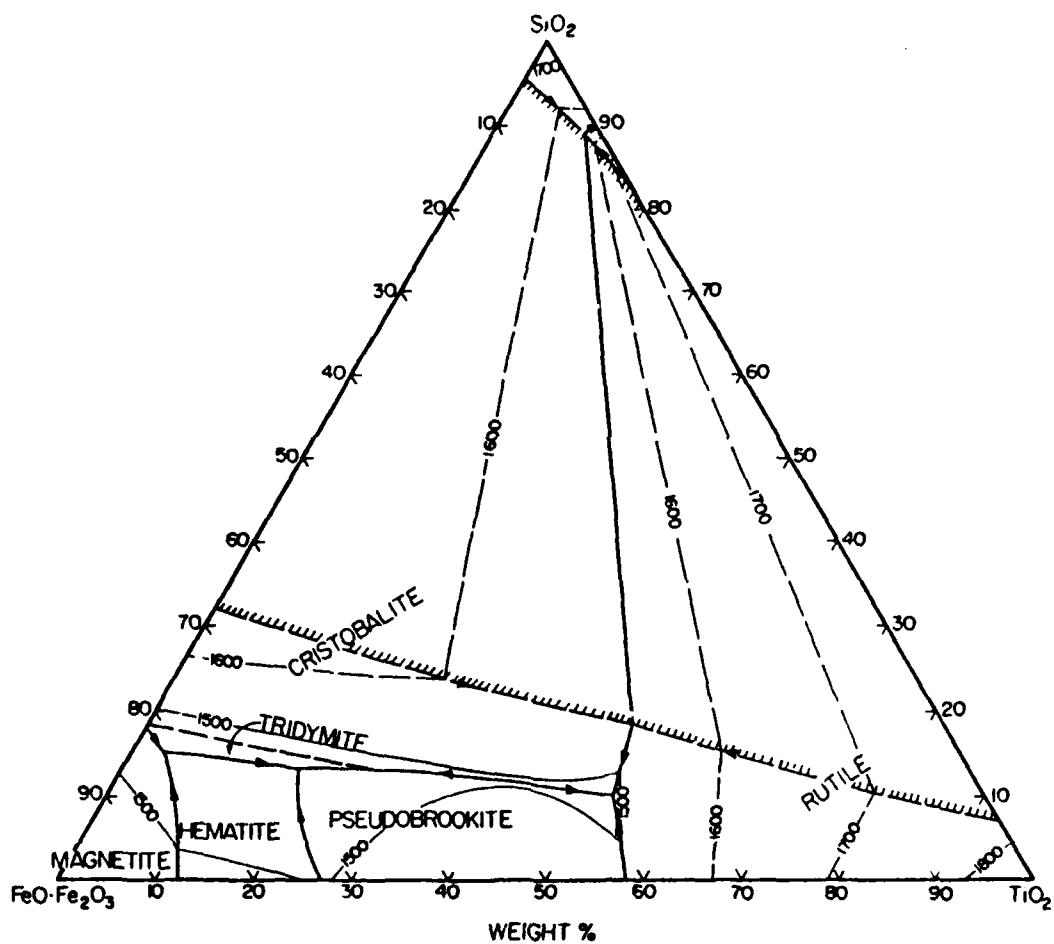
Figure E.11
Phase diagram FeO-TiO$_2$-SiO$_2$ system (Muan and Osborn, 1965, p.120).

LIST OF REFERENCES

Anderson, T.L., Hyatt, J.A. and West, J.C., "The Benefits of New High Strength Low-Alloy (HSLA) Steels," Welding Journal, v.66, September, 1987.

Annual Book of ASTM Standards, Test Methods and Analytical Procedures, Volume 3, ASTM, 1988.

Bhadeshia, H.K.D.H. and Sugden, A.A.B., "The Nonuniform Distribution of Inclusions In Low Alloy Steel Weld Deposits," Metallurgical Transactions A, v.19A, March, 1988.

Bhatti, A.R., Saggese, M.E., Hawkins, D.N., Whiteman, J.A. and Golding, M.S., "Analysis of Inclusions In Submerged Arc Welds In Microalloyed Steels," Welding Journal Research Supplement, v.63, July, 1984.

Chai, C.S. and Eagar, T.W., "Slag-Metal Equilibrium During Submerged Arc Welding," Metallurgical Transactions B, v.12B, September, 1981.

Court, S.G. and Pollard, G., "Microanalysis of Weld Metal Inclusions," Journal of Materials Science Letters, v.4, 1985.

David Taylor Naval Ship Research and Development Center Report SME-CR-07-86, Development of 100 KSI Yield Strength HSLA Steel, by T.B. Cox and A.P. Coldren, July, 1986.

David Taylor Naval Ship Research and Development Center Report SME-CR-13-86, The Metallurgy of HSLA Steel Weld Metal Produced By the Submerged Arc Process, Final Report, by D.K. Matlock and G.R. Edwards, August, 1986.

David Taylor Naval Ship Research and Development Center Report SME-88-81, Mechanisms of Strength and Toughness In a Microalloyed Precipitation Hardened Steel, by M.E. Natishan, April, 1989.

Dowling, J.M., Corbett, J.M. and Kerr, H.W., "Inclusion Phases and the Nucleation of Acicular Ferrite In Submerged Arc Welds In High Strength Low Alloy Steels," Metallurgical Transactions A, v.17A, September, 1986.

Goodman, S.R., Brenner, S.S., and Low, J.R., "An FIM-Atom Probe Study of the Precipitation of Copper From Iron-1.4 At.Pct. Copper, Part II," Metallurgical Transactions, v.4, October, 1973.

Grong, O., Siewert, T.A., Martins, G.P. and Olson, D.L., "A Model for the Silicon-Manganese Deoxidation of Steel Weld Metals," Metallurgical Transactions A, v.17A, October, 1986.

Harrison, P.L. and Farrar, R.A., "Influence of Oxygen Rich Inclusions On the Gamma-Alpha Phase Transformation In High Strength Low Alloy (HSLA) Steel Weld Metals," Journal of Materials Science, v.16, 1981.

Kiessling,R. and Lange N., Nonmetallic Inclusions In Steel, The Metals Society, London, 1978.

Kubaschewski, O., Iron Binary Phase Diagrams, Springer-Verlag, 1982.

Kuo, S., Welding Metallurgy, John Wiley and Sons, 1987.

LeMay, I. Schetky, L.M. and Krishnadev, M.R., "The Role of Copper In HSLA Steels: A Review and Update," High Strength Low Alloy Steels, South Coast Printers, 1984.

Metals Handbook, 9th ed., v.1, American Society for Metals, 1983.

Metals Handbook, 9th ed., v.6, American Society for Metals, 1983.

Miglin, M.T., Hirth, J.P., Rosenfield, A.R. and Clark, W.A.T., "Microstructure of a Quenched and Tempered, Cu-Bearing High Strength Low Alloy Steel," Metallurgical Transactions A, v.17A, May, 1986.

Muan, A. and Osborn, E.F., Phase Equilibria Among Oxides In Steelmaking, Addison Wesley Publishing, 1965.

North, T.H., Bell, H.B., Nowicki, A. and Craig, I., "Slag/Metal Interaction, Oxygen and Toughness In Submerged Arc Welding," Welding Journal Research Supplement, v.57, March, 1978.

Potkay, G.P., Microstructural Characterization of the Heat Affected Zone of HSLA-100 Steel GMA Weldment, Master's Thesis, Naval Postgraduate School, Monterey, California, December, 1987.

Reeves, M.C., "The Metallurgy of Welding of Carbon Low Alloy Steels," The Joining of Metals, Institution of Metallurgists, 1952.

Ricks, R.A., Howell, P.R. and Barrite, G.S., "The Nature of Acicular Ferrite In HSLA Steel Weld Metals," Journal of Materials Science, v.17, 1982.

BIBLIOGRAPHY

Askeland, D.R., The Science and Engineering of Materials, PWS Engineering, 1984.

Bhadeshia, H.K.D.H., Svennson, L.E. and Gretoft, B., "A Model for the Development of Microstructure in Low Alloy Steel (Fe-Mn-Si-C) Weld Deposits," Acta Metallurgica, v.33, 1985.

Clean Steel, Iron and Steel Institute Special Report No. 77, Percy Lund and Humphries and Co., 1963.

David Taylor Naval Ship Research and Development Center Report SME-CR-03-88, Effects of Varying the Austenitizing and Precipitation Hardening Temperatures and Times on the Ability of HSLA-80 to Achieve a Yield Strength of 100 KSI, by G.E. Hicho, C.H. Brady, L.C. Smith and R.J. Fields, October, 1987.

Deb, P., Challenger, K.D. and Burna, R.F., "Microstructural Characterization of Shielded Metal Arc Weldments of a Copper Bearing HSLA Steel," Materials Science and Technology, v.1, November, 1985.

Flax, R.W., Keith, R.E., and Randall, M.D., Welding the HY Steels, ASTM Defense Metals Information Center, 1971.

Gray, J.M., Ko, T., Shouhua, Z., Baurong, W. and Xishan, X., HSLA Steels, Metallurgy and Applications, ASM International, 1985.

Hussain, I., A Comparison of the Cleanliness of Steels Treated With Calcium-Silicon and Magnesium, Doctoral Thesis, School of Engineering, The Polytechinc, Wolverhampton, U.K., January, 1988.

Jessman, R.J. and Schmid, G.C., "Submerged Arc Welding A Low-Carbon Copper-Strengthened Alloy Steel," Welding Journal Welding Research Supplement, v.62, November, 1983.

Mangonon, P.L., Toughness Characterization and Specifications for HSLA and Structural Steels, The Metallurgical Society of AIME, 1977.

Metallography, ASTM Special Technical Publication 557, ASTM, 1974.

Mickleberry, K.D., Microstructural Characterization of HSLA-100 GMA Weldments, Master's Thesis, Naval Postgraduate School, Monterey, California, September, 1987.

Modin, H. and Modin, S., Metallurgical Microscopy, John Wiley and Sons, 1973.

Palm, J.H., "How Fluxes Determine The Metallurgical Properties of Submerged Arc Welds," <u>Welding Journal Welding Research Supplement</u>, v.51, July, 1972.

Reed-Hill, R.E., <u>Physical Metallurgy Principles</u>, PWS Engineering, 1973.

Widgery, D.J., "Deoxidation Practice for Mild Steel Weld Metal," <u>Welding Journal Welding Research Supplement</u>, v.55, March, 1976.

INITIAL DISTRIBUTION LIST

1. Defense Technical Information Center   2
   Cameron Station
   Alexandria, VA   22304-6145

2. Library, Code 0142   2
   Naval Postgraduate School
   Monterey, CA   93943-5002

3. Commandant of the Marine Corps   1
   Code TE 06
   Headquarters, U.S. Marine Corps
   Washington, D.C.   20380-0002

4. Dr. Alan G. Fox, Code 69Fo   1
   Department of Mechanical Engineering
   Naval Postgraduate School
   Monterey, CA   93943-5002

5. Dr. Indranath Dutta, Code 69Du   1
   Department of Mechanical Engineering
   Naval Postgraduate School
   Monterey, CA   93943-5002

6. Mr. Ernest Czyryca, Code 2814   1
   David Taylor Naval Ship Research and Development Center
   Annapolis, MD   21402-5067